Aslıhan SEZGİN

M.S. Thesis In Chemistry

January 2008

SYNTHESIS AND CHARACTERIZATION OF BORON-CONTAINING POLYMERS AND COPOLYMERS

by

Aslıhan SEZGİN

January 2008

SYNTHESIS AND CHARACTERIZATION OF BORON-CONTAINING POLYMERS AND COPOLYMERS

by

Aslıhan Sezgin

A thesis submitted to

the Graduate Institute of Science and Engineering

of

Fatih University

in partial fulfillment of the requirements for the degree of

Master of Science

in

Chemistry

January 2008
Istanbul, Turkey

APPROVAL PAGE

I certify that this thesis satisfies all the requirements as a thesis for the degree of Master of Science.

_____
Assist. Prof. Dr. Metin TÜLÜ
Head of Department

This is to certify that I have read this thesis and that in my opinion it is fully adequate, in scope and quality, as a thesis for the degree of Master of Science.

_____
Assist. Prof. Dr. Abdülhadi BAYKAL
Supervisor

This is to certify that I have read this thesis and that in my opinion it is fully adequate, in scope and quality, as a thesis for the degree of Master of Science.

_____
Assoc. Prof. Dr. Ayhan BOZKURT
Cosupervisor

Examining Committee Members

Prof. Dr. Naz Mohammed AGH ATABAY _____

Assoc. Prof. Dr. Ayhan BOZKURT _____

Assist. Prof. Dr. Abdülhadi BAYKAL _____

It is approved that this thesis has been written in compliance with the formatting rules laid down by the Graduate Institute of Sciences and Engineering.

_____
Assist. Prof. Dr. Nurullah ARSLAN
Director

January 2008

SYNTHESIS AND CHARACTERIZATION OF BORON-CONTAINING POLYMERS AND COPOLYMERS

Aslıhan Sezgin

M. S. Thesis - Chemistry
January 2008

Supervisor: Assist. Prof. Dr. Abdülhadi BAYKAL

ABSTRACT

Proton conduction in novel anhydrous membranes based on inorganic host polymer, poly(4-vinylbenzeneboronic acid), PVBBA and phosphoric acid, H_3PO_4 as proton solvent was studied. The composite materials were prepared by the insertion of the proton solvent into PVBBA at different stoichiometric ratios to get PVBBA$(H_3PO_4)_x$ composite electrolytes. Homopolymer and the composite materials were characterized by FT-IR and ^{11}B MAS-NMR. Thermogravimetric analysis (TGA) illustrated that the composite materials are thermally stable up to approximately 140 ^{o}C. An exponential weight loss above this temperature was attributed to self-condensation of boric acid units. Differential scanning calorimetry (DSC) results proved the softening effect of the proton solvent. The temperature dependence of the proton conductivity was modeled with Arrhenius relation. PVBBA$(H_3PO_4)_2$ has a maximum proton conductivity of 0.0013 S/cm at RT and 0.005 S/cm at 80 ^{o}C. Poly(4-VBBA-co-4-VIm) copolymers were synthesized by copolymerization of the monomers 4-vinylbenzeneboronic acid, VBBA and 4-vinylimidazole, 4-VIm at various monomer feed ratios by free-radical polymerization. The copolymers were characterized by ^{13}C NMR, and poly(4-VBBA-co-4-VIm) composition was determined by elemental analysis. The proton exchange reaction between acid and heterocycle is confirmed by FT-IR. Thermal properties of the samples were investigated via TGA and DSC. The morphology of the copolymers was characterized by X-ray powder diffraction (XRD). Proton conductivity of the copolymers increased with the doping ratio and reached to 0.0027 S/cm for poly(4-VBBA-co-4-VIm)$(H_3PO_4)_2$.

Poly(glycidyl methacrylate) (PGA) was synthesized via radical polymerization of glycidyl methacrylate (GMA) initiated by 2,2-azobisisobutyronitrile (AIBN) and followed by modification with ethanolamine. Borate-loaded PGMAN (PGMANB) complexes were prepared by mixing PGMAN and boric acid solution in a molar ratio of 1:1. PGMANB was investigated by FT-IR spectroscopy, elemental analysis and ^{11}B MAS-NMR to confirm the structure and its thermal properties were studied by TGA.

Keywords: Poly(4-vinylbenzeneboronic acid), 4-vinylimidazole, copolymer, polymer electrolyte, phosphoric acid, anhydrous proton conductivity, thermal properties, boric acid, FT-IR, ^{11}B MAS-NMR.

BOR İÇEREN POLİMER VE KOPOLİMERLERİN SENTEZİ VE KARAKTERİZASYONU

Aslıhan Sezgin

Yüksek Lisans Tezi - Kimya
Ocak 2008

Tez yöneticisi: Assist. Prof. Dr. Abdülhadi BAYKAL

ÖZ

Nemsiz ortamda yeni proton iletken membranlar, anorganik host polimer, poli(4-vinilbenzenboronik asit), PVBBA, proton solvent fosforik asitle, H_3PO_4 çalışılmıştır. PVBBA$(H_3PO_4)_x$ elektrolitleri farklı stokiometrik oranlarda proton solvent ilave edilerek hazırlanmıştır. Homopolimer ve elektrolitler FT-IR spektroskopi ve ^{11}B MAS-NMR yardımıyla karakterize edilmiştir. Termal ağırlık analiz (TGA) sonuçları kompozitlerin termal kararlılığının 140 ^{o}C'ye ulaştığını göstermektedir.Bu sıcaklığın üzerinde görülen üssel kütle kaybı borik asit ünitelerindeki yoğunlaşmadan kaynaklanmaktadır. Diferansiyel taramalı kalorimetre (DSC) sonuçları proton solventin yumuşatıcı etkisini ispatlamaktadır. Arrhenius eşitliğiyle sıcaklığa bağlı proton iletkenliği modellenmiştir. PVBBA$(H_3PO_4)_2$ oda sıcaklığında 0.0013 S/cm ve 80 ^{o}C'de ise 0.005 S/cm gibi maksimum iletkenlikler göstermiştir. Poly(4-VBBA-co-4-VIm) kopolimerleri, 4-vinilbenzenboronik asit, VBBA ve 4-vinilimidazol, 4-VIm monomerleri farklı oranlarda kullanılarak free radikal polimerizasyon yöntemiyle sentezlenmiştir. Kopolimerler ^{13}C NMR'le karakterize edilmiştir. Bileşenleri elemental analiz sonuçlarıyla tespit edilmiştir. Heterohalka ve asit arasındaki etkileşim FT-IR spektroskopi yardımıyla araştırılmıştır. Numunelerin termal özellikleri TGA ve DSC yöntemleri kullanılarak aydınlatılmıştır. Kopolimerlerin morfolojisi X-Işını difraksiyonu yöntemiyle karakterize edilmiştir. Kopolimerlerin proton iletkenliği, asit içeriğiyle artmaktadır ve nemsiz poli(4-VBBA-co-4-VIm)$(H_3PO_4)_2$ için 0.0027 S/cm olarak ölçülmüştür.

Poli(glisidilmetakrilat) (PGMA) radikalik polimerizasyon yöntemiyle GMA monomerinden 2,2-azobisizobütironitril (AIBN) başlatıcısı kullanılarak sentezlenip etanolaminle modifiye edilmiştir. Etanolaminle modifiye edilmiş PGMAN polimeri,

1:1 mol oranında hazırlanmış borik asit çözeltisiyle karıştırılarak PGMANB kompleksi elde edilmiştir. Elemental analiz, FT-IR ve ^{11}B MAS-NMR ile PGMANB kompleksinin yapısı incelenip TGA kullanılarak termal özellikleri çalışılmıştır.

Anahtar Kelimeler: Poli(4-vinilbenzenboronik asit), 4-vinilimidazol, kopolimer, fosforik asit, polimer elektrolit, nemsiz proton iletkenlik, termal özellikler, boric asit, FT-IR, ^{11}B MAS-NMR.

ACKNOWLEDGMENT

First of all, I would like to thank my thesis supervisor Assist. Prof. Dr. Abdülhadi BAYKAL and cosupervisor Assoc. Prof. Dr. Ayhan BOZKURT. Their motivation and power kept me doing all the work. Their academic activities will be references in my future studies.

This work is supported by TÜBİTAK under the contract number 105M345.

I would like to thank Research Assistant Sevim Ünügür ÇELİK for her kind help.

I would like to thank Research Assistant Ümit AKBEY for studying ^{11}B MAS-NMR and ^{13}C NMR in the Max-Planck Institute for Polymer Research, Mainz, Germany, where part of the characterizations were carried out.

Finally, I would like to thank my parents for their love, patience and encouragement.

TABLE OF CONTENTS

LIST OF TABLES

TABLES

LIST OF FIGURES

FIGURE

LIST OF ABBREVATIONS

ABBREVATIONS

PEMFC	Polymer Electrolyte Fuel Cell
PVBBA	Poly(4-Vinylbenzeneboronic acid)
AIBADC	α,α'– Azodiisobutyramidin Dihydrochlorid purum
VBBA	4-Vinylbenzeneboronic acid,
PGMA	Poly(glycidyl methacrylate)
GMA	Glycidyl methacrylate
AIBN	2,2-azobisisobutyronitrile
PGMAN	Ethanolamine modificated PGMA
PGMANB	Borate-loaded PGMAN
PEFC	Polymer Electrolyte Fuel Cell
AFC	Alkaline Fuel Cell
PAFC	Phosphoric Acid Fuel Cell
MCFC	Molten Carbonate Fuel Cell
ITSOFC	Intermediate Temperature Solid Oxide Fuel Cell
TSOFC	Tubular Solid Oxide Fuel Cell
PEM	Polymer Electrolyte Membrane, Proton Exchange Membrane
MCFC	Molten Carbonate Fuel Cell
ITSOFC	Intermediate Temperature Solid Oxide Fuel Cell
TSOFC	Tubular Solid Oxide Fuel Cell
PEM	Polymer Electrolyte Membrane, Proton Exchange Membrane
IEC	Ion Exchange Capacity
RH	Relative Humidity
MEA	Membrane Electrode Assembly
PBI	Polybenzimidazole

PEO	Polyethyleneoxide
PFG-NMR	Pulsed Field Gradient Nuclear Magnetic Resonance
BPEI	Branched Polyethylene Imine
CPMD	Car-Parrinello Molecular Dynamics
PFSA	Perfluorosulfonic acid
$PhB(OH)_2$	Phenylboronic acid
ORTEP	Oak Ridge Thermal Ellipsoid Plot
AcPBA	3-acrylamidophenyl-boronic acid
LCST	Lower Critical Solution Temperature
Imi	Imidazole
P4-VIm	Poly(4-vinylimidazole)
VPA	Vinylphosphonic acid
4-VIm	4-vinylimidazole or 4(5)-vinylimidazole
PAMPSA	Poly(2-acrylamido-2-methyl-1-propanesulfonic acid)
AA	Adibic acid
BIm	Benzimidazole
PAA	Polyacrylic acid
PVBBA	Poly(4-Vinylbenzeneboronic acid)
4-VBBA	4-vinylbenzeneboronic acid
PTFE	Polytetrafluoroethylene
UA	Urocanic acid
VTF	Vogel-Tamman–Fulcher-type

CHAPTER 1

INTRODUCTION

Proton conducting polyelectrolyte membranes have received a great deal of attention due to their promissing applications as polymer electrolyte fuel cells (PEMFC) (Blomen and Mugerwa, 1993). At present, fluorinated polyelectolyte membranes, such as Nafion, Flemion, and Aciplex, were generally used for the solid electrolyte membranes of PEMFC, because they have excellent chemical thermal stability, and high proton conductivity. These membranes, however, have crucial problems that hinder efforts to commercialize profitable PEMFC and also to develop PEMFC that can operate at high power density and high temperature. The serious problem that must be overcome as soon as possible are the high cost and low recycling properties, which are attributed to the perfluorinated polymer backbones (Rikukawa et al., 2005).

However, the boiling point of water limits the usage of water as a proton solvent at high temperature. H_3PO_4, due to the formation of polyphosphoric acid network for proton transport at high temperatures and anhydrous environment, is the best solvent for proton transport at high temperatures and anhydrous conditions. It has been demonstrated that in highly viscous anhydrous phosphoric acid, 98% of the total conductivity arises from structure diffusion of proton (Kreuer et al., 1993).

The copolymerization of heterocyclic monomers with proton donating monomers was thought to produce promising materials to employ as high temperature membranes where both acidic units and heterocycles may act as ‘‘proton solvent’’. A comparison of the proton conductivities of copolymers that contain similar acidic and basic units immobilized in the backbone with inorganic-organic hybrid membranes is also interesting (Bozkurt et al., 2003). These heterocycles form hydrogen bonded networks

and proton transport occurs by hop-turn mechanism via structure diffusion. Although these proton solvents are widely used in closed electrochemical cells, such as supercapacitators and electrochemical devices, the volatility of the heterocycles prevents them from being used in open electrochemical systems, such as fuel cells. Therefore, the use of heterocycles as the proton solvent requires their immobilisation in the polymer membrane in such a way that high mobility of the protonic charge carriers is still provided (Kreuer, 2001).

This work focus on understanding fundamental properties of acid doped poly(4-vinylbenzeneboronic acid), PVBBA homopolymer and poly(4-VBBA-co-4-VIm) copolymers. There is a new host matrix, poly(4-vinylbenzeneboronic acid), PVBBA which was produced by free radical solution polymerization of 4-vinylbenzeneboronic acid using α,α'-azodiisobutyramidine dihydrochloride purum (AIBADC) as initiator. Then PVBBA was doped with phosphoric acid at several stoichiometric ratios. The properties of the membranes were investigated by FT-IR, TGA and DSC. Proton conductivity of anhydrous electrolytes was measured via impedance spectroscopy. Poly(4-VBBA-co-4-VIm) copolymers were synthesized by copolymerization of the monomers 4-vinylbenzeneboronic acid, VBBA and 4-vinylimidazole), 4-VIm at various monomer feed ratios by free-radical polymerization. The copolymers were characterized by ^{13}C NMR, and the copolymer composition was determined via elemental analysis. The membrane properties of these copolymers were investigated after doping with phosphoric acid at several stoichiometric ratios. The proton exchange reaction between acid and heterocycle is confirmed by FT-IR. Thermal properties of the samples were investigated via Thermogravimetric analysis (TGA) and Differential scanning calorimetry (DSC). The morphology of the copolymers was characterized by X-ray powder diffraction (XRD). The temperature dependence of proton conductivities of the samples was investigated by means of impedance spectroscopy. The membrane properties of the copolymers are investigated after doping them with phosphoric acid at different compositions. Boronic acid units acted as crosslinker (Senel et al., 2007) and both proton solvents (immobilized imidazole and phosphoric acid) were used as proton charge carries. The thermal and anhydrous proton conductivity properties are investigated and compared with previously reported systems.

Poly(glycidyl methacrylate) (PGMAN) was synthesized via radical polymerization of glycidyl methacrylate (GMA) initiated by 2,2’-azobisisobutyronitrile (AIBN) and followed by modification of with ethanolamine. Borate-loaded PGMAN (PGMANB) complexes were prepared by mixing PGMAN and boric acid solution in a molar ratio of 1:1. PGMANB was investigated by FT-IR spectroscopy, elemental analysis and ^{11}B MAS-NMR to confirm the structure and its thermal properties were studied by thermogravimetry analysis.

CHAPTER 2

APPLICATION OF PROTON CONDUCTING ELECTROLYTES FUEL CELLS

Fuel cells are electrochemical devices that convert the chemical energy of a reaction directly into electrical energy. The basic physical structure or building block of a fuel cell consists of an electrolyte layer in contact with a porous anode and cathode on either side. A schematic representation of a fuel cell with the reactant/product gases and the ion conduction flow directions through the cell is shown in Fig. 2.1.

In a typical fuel cell, gaseous fuels are fed continuously to the anode (negative electrode) compartment and an oxidant (i.e., oxygen from air) is fed continuously to the cathode (positive electrode) compartment; the electrochemical reactions take place at the electrodes to produce an electric current. A fuel cell, although having components and characteristics similar to those of a typical battery, differs in several respects. The battery is an energy storage device. The maximum energy available is determined by the amount of chemical reactant stored within the battery itself. The battery will cease to produce electrical energy when the chemical reactants are consumed (i.e., discharged). In a secondary battery, the reactants are regenerated by recharging, which involves putting energy into the battery from an external source. The fuel cell, on the other hand, is an energy conversion device that theoretically has the capability of producing electrical energy for as long as the fuel and oxidant are supplied to the electrodes.

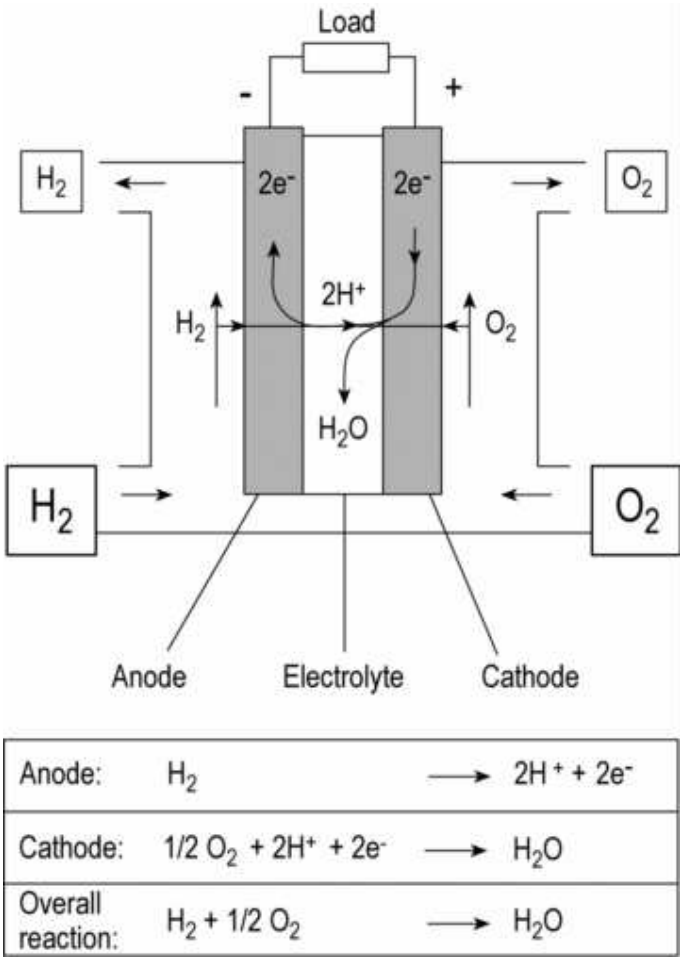

Figure 2.1. Schematic illustration of an individual fuel cell (Cremers and Stimming, 2004).

Fig. 2.1 is a simplified diagram that demonstrates how the fuel cell works. In reality, degradation, primarily corrosion, or malfunction of components limits the practical operating life of fuel cells. Note that the ion specie and its transport direction can differ, influencing the site of water production and removal, a system impact. The ion can be either a positive or a negative ion, meaning that the ion carries either a positive or negative charge (surplus or deficit of electrons). The fuel or oxidant gases flow past the surface of the anode or cathode opposite the electrolyte and generate electrical energy by the electrochemical oxidation of fuel, usually hydrogen, and the electrochemical reduction of the oxidant, usually oxygen (Fuel Cell Handbook, 2000).

A variety of fuel cells are in different stages of development. They can be classified by use of diverse categories, depending on the combination of type of fuel and oxidant, whether the fuel is processed outside (external reforming) or inside (internal reforming) the fuel cell, the type of electrolyte, the temperature of operation, whether the reactants are fed to the cell by internal or external manifolds, etc. The most common classification of fuel cells is by the type of electrolyte used in the cells and includes; polymer electrolyte fuel cell (PEFC), alkaline fuel cell (AFC), phosphoric acid fuel cell (PAFC), molten carbonate fuel cell (MCFC), intermediate temperature solid oxide fuel cell (ITSOFC), and tubular solid oxide fuel cell (TSOFC). These fuel cells are listed in the order of approximate operating temperature, ranging from ~80 ^{o}C for PEFC, ~100 ^{o}C for AFC, ~200 ^{o}C for PAFC, ~650 ^{o}C for MCFC, ~800 ^{o}C for ITSOFC, and 1000 ^{o}C for TSOFC. The operating temperature and useful life of a fuel cell dictate the physicochemical and thermomechanical properties of materials used in the cell components (i.e., electrodes, electrolyte, interconnect, current collector, etc.). Aqueous electrolytes are limited to temperatures of about 200 ^{o}C or lower because of their high water vapor pressure and/or rapid degradation at higher temperatures. The operating temperature also plays an important role in dictating the type of fuel that can be used in a fuel cell. The low-temperature fuel cells with aqueous electrolytes are, in most practical applications, restricted to hydrogen as a fuel. In high-temperature fuel cells, CO and even CH_4 can be used because of the inherently rapid electrode kinetics and the lesser need for high catalytic activity at high temperature. However, descriptions later in this section note that the higher temperature cells can favor the conversion of CO and CH_4 to hydrogen, then use the equivalent hydrogen as the actual fuel (Fuel Cell Handbook, 2000).

2.1 Polymer Electrolyte Fuel Cell (PEFC)

Fuel cells may become the energy-delivery devices of the 21st century. Although there are many types of fuel cells, polymer electrolyte membrane (also termed “Proton Exchange Membrane”) (PEM) fuel cells are being developed for three main application: automotive, stationary, and portable power. Each of these applications has its unique operating conditions and material requirements. As shown in Fig. 2.2, a PEMFC consists of two electrodes and a solid polymer membrane, which acts as an electrolyte.

The polymer electrolyte membrane is sandwiched between two platinum-porous electrodes such as an carbon paper and mesh (Rikukawa and Sanui, 2000).

The working principle of hydrogen PEM fuel cell is often described as reverse electrolysis. The hydrogen fuel is supplied to the anode electrode. The following reaction takes place at anode, accelerated by a platinum catalyst:

Anode: $H_2 \rightarrow 2H^+ + 2e^-$

The protons (H^+) migrate through the Polymer Electrolyte Membrane (PEM) to the cathode. At cathode, a reaction takes place with oxygen from air:

Cathode: $O_2 + 4\ H^+ + 4e^- \rightarrow 2\ H_2O$

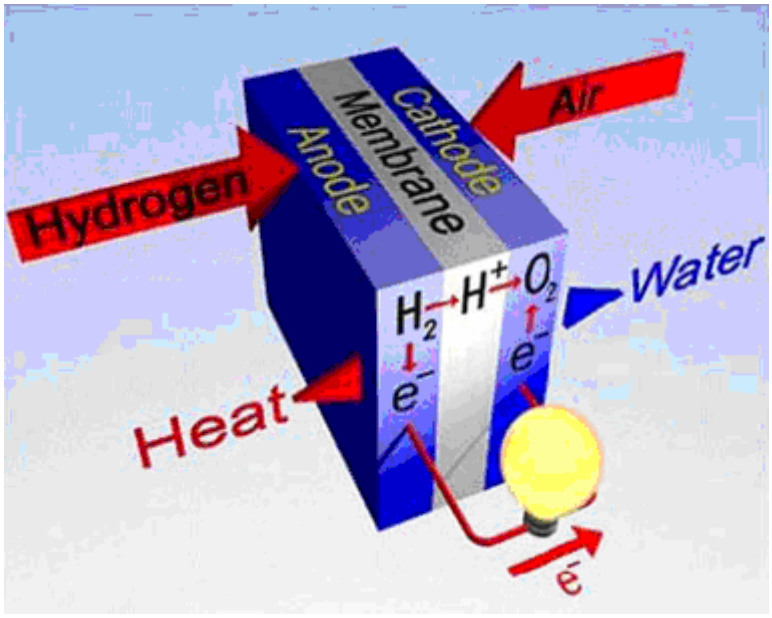

Figure 2.2. Polymer Electrolyte Membrane Fuel Cell (PEMFC) (Sukumar, 2006).

Notably, the electrons are required for the cathode reaction to produce water. But the electrolyte membrane, which separates the cathode and the anode, is permeable only for protons. Therefore, the electrons have to travel through an external circuit to the cathode.

Overall reaction: $2\ H_2 + O_2 \rightarrow 2\ H_2O$ + Electrical energy + Heat

2.2 Alkaline Fuel Cell (AFC)

Alkaline fuel cells use an aqueous solution of potassium hydroxide (KOH) in a porous stabilized matrix as an electrolyte (Fig. 2.3). The concentration of KOH can be varied with the fuel cell operating temperature, which ranges from 65 °C to 220 °C (Sukumar, 2006). The electrolyte is retained in a matrix (usually asbestos), and a wide range of electrocatalysts can be used (e.g., Ni, Ag, metal oxides, spinels, and noble metals). The fuel supply is limited to non-reactive constituents except for hydrogen. CO is a poison, and CO_2 will react with the KOH to form K_2CO_3, thus altering the electrolyte. Even the small amount of CO_2 in air must be considered with the alkaline cell (Fuel Cell Handbook, 2000).

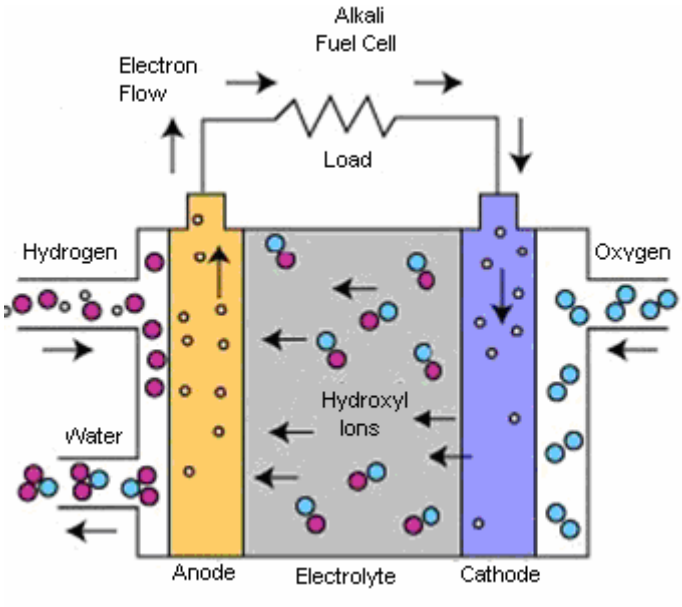

Figure 2.3. Alkaline Fuel cell (AFC) (Sukumar, 2006).

Anode Reaction: $2\ H_2 + 4\ OH^- \rightarrow 4\ H_2O + 4\ e^-$

Cathode Reaction: $O_2 + 2\ H_2O + 4\ e^- \rightarrow 4\ OH$

Overall Net Reaction: $2\ H_2 + O_2 \rightarrow 2\ H_2O$

2.3 Phosphoric Acid Fuel Cell (PAFC)

A phosphoric acid fuel cell (PAFC) consists of an anode and a cathode made up of finely dispersed platinum catalyst on carbon paper-, and a silicon carbide matrix that holds the phosphoric acid electrolyte. The operating temperature of the fuel cell would be around 150 to 200 °C. The high operating temperature of PAFC can tolerate a CO concentration of about 1.5 percent due to concentrated phosphoric acid (as an electrolyte), which makes PAFC to operate above the boiling point of water, a limitation on other acid electrolytes that require water for conductivity.

The PAFC reactions that occur are:

Anode: $H_2 \rightarrow 2H^+ + 2e^-$

Cathode: $O_2 + 4\,H^+ + 4e^- \rightarrow 2\,H_2O$

At the anode, hydrogen is split into two hydrogen ions (H^+) and two electrons, pass to the cathode via electrolyte and via the external circuit (electric load). At the cathode, water is formed and eventually eliminated as shown in the Fig. 2.4.

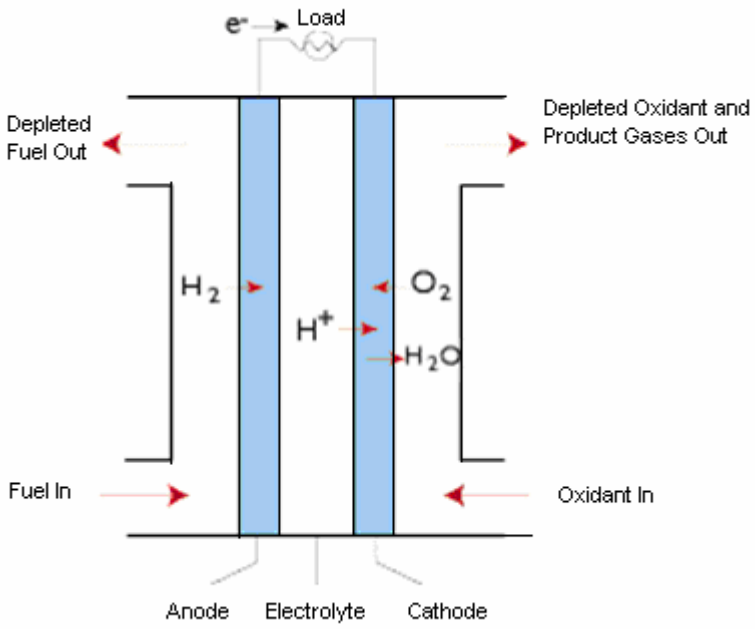

Figure 2.4. Phosphoric Acid Fuel Cell (Sukumar, 2006).

This is the most commercially developed type of fuel cell and is being used in hotels, hospitals, and office buildings. The phosphoric acid fuel cell can also be used in heavy automobiles (Sukumar, 2006).

2.4 Molten Carbonate Fuel Cell (MCFC)

The electrolyte in this fuel cell is usually a combination of alkali carbonates, which is retained in a ceramic matrix of $LiAlO_2$. The fuel cell operates at 600-700 ^oC where the alkali carbonates form a highly conductive molten salt, with carbonate ions providing ionic conduction. At the high operating temperatures in MCFCs, Ni (anode) and nickel oxide (cathode) are adequate to promote reaction. Noble metals are not required (Fuel Cell Handbook, 2000).

The MCFC reactions that occur are:

Anode reaction: $H_2 + CO_3^{2-} \rightarrow H_2O + CO_2 + 2e^-$

$CO + CO_3^{2-} \rightarrow 2CO_2 + 2e^-$

Cathode reaction: $O_2 + 2CO_2 + 4\ e^- \rightarrow 2CO_3^{2-}$

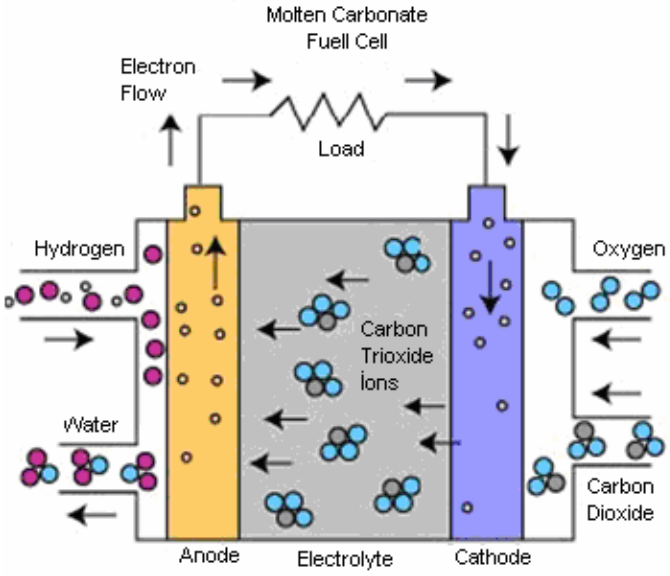

Figure 2.5. Molten Carbonate Fuel Cell (Sukumar, 2006).

The anode process involves a reaction between hydrogen and carbonate ions (CO_3^{2-}), which produces water and carbon dioxide (CO_2), while releasing electrons to the anode. The cathode combines oxygen and CO_2 from the oxidant stream with electrons to produce carbonate ions, which enter the electrolyte. The need for CO_2 in the oxidant stream requires a system for collecting CO_2 from the anode exhaust and mixing it with the cathode feed stream (Fig. 2.5) (Sukumar, 2006).

2.5 Solid Oxide Fuel Cells (SOFC)

Solid oxide fuel cell (SOFC) uses hard ceramic as an electrolyte, which operates at temperatures up to 1000 °C. Solid oxide fuel cells (SOFC) that are currently under development use a thin layer of stabilized zirconia (zirconium oxide) as a solid ceramic electrolyte-, along with a lanthanum manganate cathode and a nickel-zirconia anode. In operation, hydrogen or carbon monoxide (CO) in the fuel stream reacts with oxide ions (O^{2-}) at the electrolyte to produce water or CO_2. In the course of reactions, the electrons are generated and then, travel towards cathode via the external load and get converted into oxide ion. Notably, both CO and H_2 can be used as energy source in solid oxide fuel cell (Fig. 2.6).

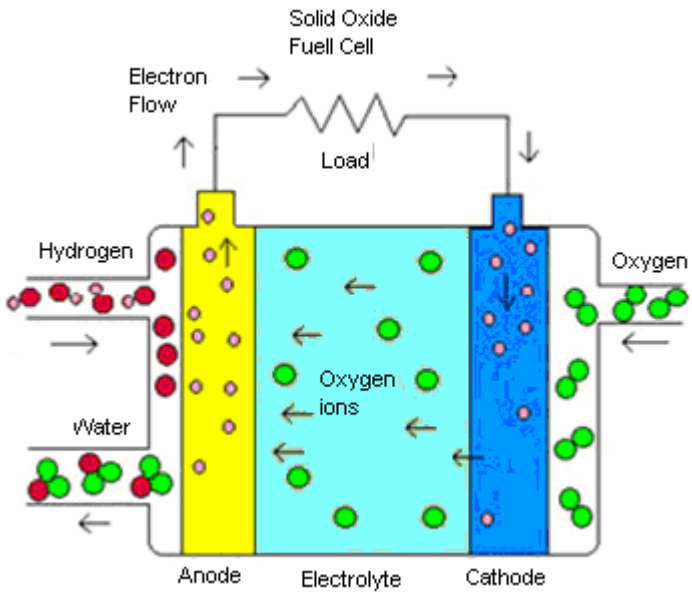

Figure 2.6. Solid Oxide Fuel Cell (Sukumar, 2006).

The SOFC reactions that occur include:

Anode reaction: $H_2 + O^{2-} \rightarrow H_2O + 2\ e^-$

$CO + O^{2-} \rightarrow CO_2 + 2\ e^-$

$CH_4 + 4\ O^{2-} \rightarrow 2\ H_2O + CO_2 + 8\ e^-$

Cathode reaction: $O_2 + 4\ e^- \rightarrow 2\ O^{2-}$

This fuel cell is a promising option for high-powered applications, such as industrial uses or central electricity generating stations (Sukumar, 2006). In low-temperature fuel cells (PEFC, AFC, PAFC), protons or hydroxyl ions are the major charge carriers in the electrolyte, whereas in the high-temperature fuel cells, MCFC, ITSOFC, and TSOFC, carbonate ions and oxygen ions are the charge carriers, respectively. Major differences between the various cells are shown in Table 2.1 (Fuel Cell Handbook, 2000).

Table 2.1 Summary of Major Differences of the Fuel Cell Types (Fuel Cell Handbook, 2000)

	PEFC	**AFC**	**PAFC**	**MCFC**	**ITSOFC**	**TSOFC**
Electrolyte	Ion Exchange Membranes	Mobilized or Immobilized Potassium Hydroxide	Immobilized Liquid Phosphoric Acid	Immobilized Liquid Molten Carbonate	Ceramic	Ceramic
Operating Temperature	80°C	65-220°C	205°C	650°C	600-800°C	800-1000°C
Charge Carrier	H^+	OH^-	H^+	CO_3^{2-}	O^{2-}	O^{2-}
External Reformer for CH_4 (below)	Yes	Yes	Yes	No	No	No
Prime Cell Components	Carbon-based	Carbon-based	Graphite-based	Stainless-based	Ceramic	Ceramic
Catalyst	Platinum	Platinum	Platinum	Nickel	Perovskites	Perovskites
Product Water Management	Evaporative	Evaporative	Evaporative	Gaseous Product	Gaseous Product	Gaseous Product
Product Heat Management	Process Gas + Independent Cooling Medium	Process Gas + Electrolyte Calculation	Process Gas + Independent Cooling Medium	Internal Reforming + Process Gas	Internal Reforming + Process Gas	Internal Reforming + Process Gas

The most successful membrane is the Nafion membrane, which was developed initially by Dupont in 1960's. This membrane offers quite good performance below 90 ^{o}C under fully hydrated conditions. It has high conductivity (>0.05 S/cm at room temperature and 100% relative humidity) although the content of sulfonic group is low (ion exchange capacity = 0.9). Also, it has good chemical and mechanical stability due to the perfluorinated main chain. However, the proton conductivity of Nafion is dependent on the presence of water to solvate the proton of the sulfonic acid groups. Consequently, the operational temperature is limited to below 100 ^{o}C, typically 50-90 ^{o}C, at ambient pressure. For a good membrane to be used for high temperature PEMFC, it should have the following material characteristics (Ma Y., 2004):

- High proton conductivity (>0.001 S/cm, prefer to >0.01 S/cm, more preferable >0.1 S/cm), to support high currents with minimal resistive losses, and zero electronic conductivity.
- Good thermal stability (thermally stable up to 150 ^{o}C, with no hydrolysis at high temperature and low degree of hydration).
- Good mechanical strength and stability at fuel cell operating conditions, i.e. free standing membrane with small swelling degree under different relative humidities, strong enough for preparation of membrane electrode assembly (MEA).
- Chemical and electrochemical stability at fuel cell operating conditions.
- Good barrier for reactant species (H_2, O_2, small organic fuels such as methanol), important for minimizing coulombic efficiency loss.
- High electrolyte transport, to maintain uniform electrolyte content and to prevent localized vacancy.
- Good chemical compatibility in fuel cell environment, good processibility for preparation of MEA.
- Low cost.

Based on the classification of proton solvents, there are three basic approaches to high temperature PEMs (Ma Y., 2004):

(a) Membranes that use water as proton carrier. Efforts have been made at retaining water in the membrane at higher temperatures.
(b) Anhydrous proton-conducting polymers where the proton is transferred not through water, but through other proton solvents such as phosphate ion (H_4PO^{4+} and H_2PO^{4-}) (e.g. polybenzimidazole/H_3PO_4 system at high temperature and low relative humidity) (Wainright et al., 1995), imidazole (e.g. sPEEK/imidazole system (Kreuer et al., 1998)), and sulfamide (e.g. sulfamide/PEO/guanidine system (Bermudez et al., 1992)).
(c) Membrane where the proton transport involves mixture of two proton solvents, such as water and phosphate ions.

Three ways of achieving high temperature membranes have been proposed :

(i) membranes made of new ionomers exhibiting the desired characteristics;
(ii) membranes in which suitable oxygenated acids (e. g. phosphoric or sulfuric acids) are solubilized in a polymeric matrix bearing basic groups (e.g. PBI);
(iii) inorganic /organic composite membranes.

CHAPTER 3

PROTON CONDUCTION MECHANISMS

A proton conductor is an electrolyte, typically a solid electrolyte, in which movable hydrogen ions (protons) are the primary charge carriers. Proton conductors are usually composed of polymer or ceramic because the pore size is small enough that larger negative ions are locked into the solid matrix, and only very small ions (positive hydrogen ions - bare protons) can participate in a direct current. Proton conductors are usually solid materials. When in the form of thin membranes, proton conductors are an essential part of small, inexpensive fuel cells.

Proton conduction was first suggested by Alfred Rene Jean Paul Ubbelohde and S.E. Rogers. Water is the best solvent for protons and exhibits unusually high equivalent conductivity of protons, which exceeds the hydrodynamic limit by a factor of 4.5 under ambient conditions. The process for proton transport in water is explained by “Grotthuss mechanism" (Grotthuss, 1806; Kreuer, 1997) also called “hopping mechanism” or “chain mechanism” or “structure diffusion”. The proton transport comprises rapid intermolecular proton transfers (Hopping) down a chain of hydrogen bonds where the transfer events are assumed to be highly correlated, and reorientation of water dipoles in order to produce a configuration which allows for the next hopping event (Kreuer, 1997).

The first process leads to a polarization of the hydrogen bond chain, i.e. to a local relative charge displacement, but not to dc conductivity. The second process causes the depolarization of the chain by reorientation of the water dipoles (Fig. 3.1).

The mechanism of proton migration in water has been studied extensively (Eigen, 1964; Agmon, 1995; Agmon, 1996). Basically, for a fast Grotthuss type mechanism, it must enable the formation of protonic defects and provide strongly fluctuating proton donor and acceptor functions in an otherwise non-polar environment. The latter avoids strong solvent effects that tend to suppress proton transfer reactions (Kreuer, 1997; Kreuer, 1996).

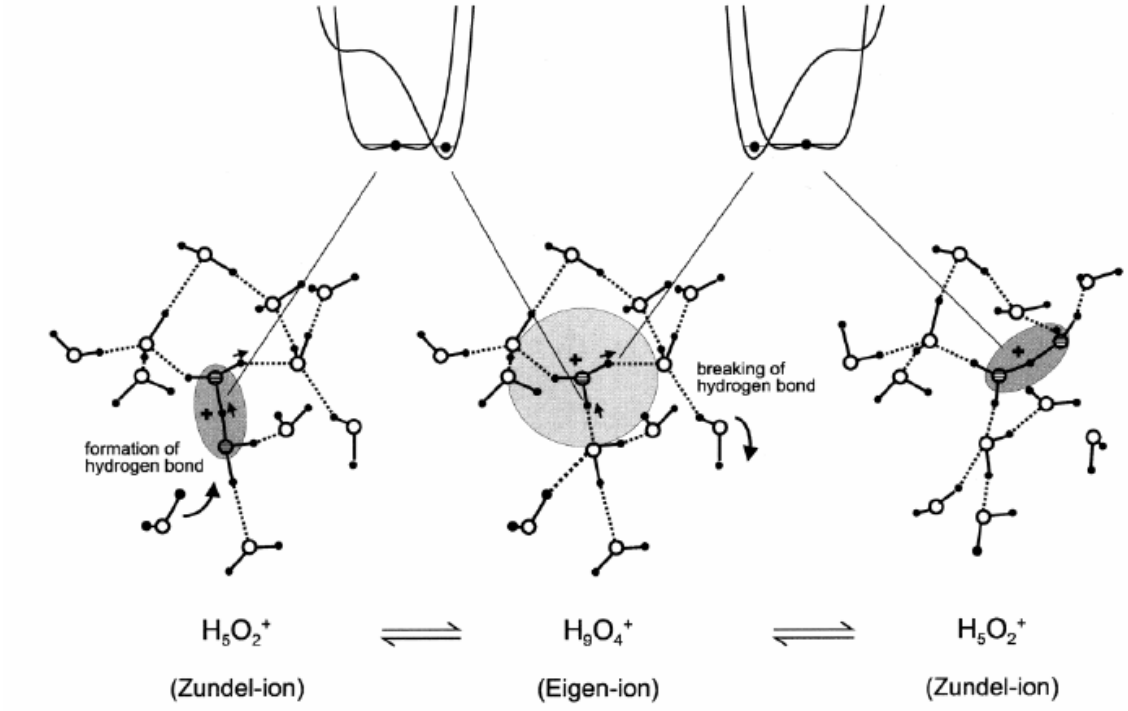

Figure 3.1. Proton transfer in H_2O molecules (Kreure et al., 2004).

However, this mechanism cannot explain all abnormal proton conductive systems. Based on NMR spectra and self-diffusion coefficients, Kreuer et al. (Kreuer et al., 1982) proposed “Vehicle Mechanism”, also called molecular diffusion, for the interpretation of the conductivity of fast proton conductors such as zeolites, Nafion etc. According to this model the proton does not migrate as H^+ but as H_3O^+, NH_4^+, etc., bonded to a “ vehicle” such as H_2O, NH_3, etc. (Fig. 3.2) The “unloaded” vehicles move in the opposite direction. Hydrogen bond is not necessary for proton transport with this model.

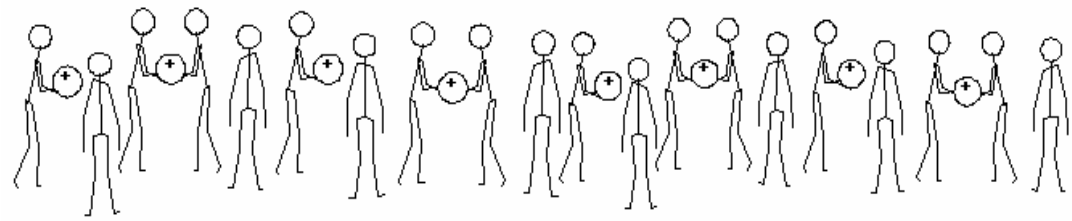

Grotthuss Mechanism

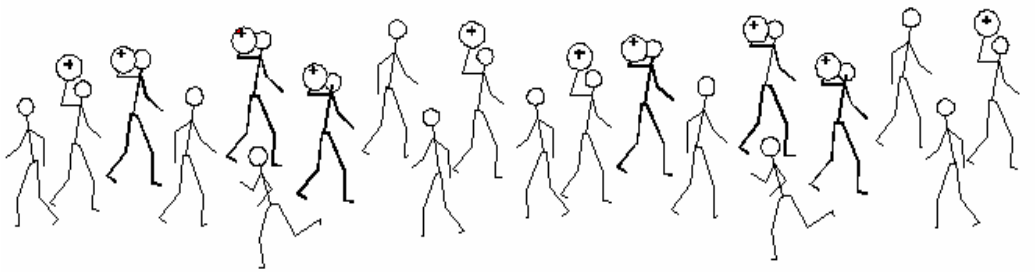

Vehicle Mechanism

Figure 3.2. Schematic representation of phenomena involved in proton conduction mechanisms (Kreuer et al., 1982).

In some systems, the conduction mechanism is contributed by these two models together. Also, the conduction mechanism can change from one model to another model based on the temperature and concentration of the system. For example, in concentrated aqueous solutions of acids such as aqueous HCl, the proton conduction can be well explained by vehicle mechanism. However, if the acid solutions are diluted, i.e. increasing solvent (H_2O) concentration, there is an increasing contribution of structure diffusion to the overall conductivity, i.e. both of the mechanisms (the mixed mechanism) exist for proton conduction. Kreuer distinguished the molecular diffusion (vehicle mechanism) and structure diffusion (Grotthuss mechanism) of proton by measuring the self-diffusion coefficients by means of the PFG-NMR technique. Basically, in anhydrous oxo-acids such as H_3PO_4 solid acidic salts of oxo-acids such as $CsHSO_4$ and $Zr(HPO_4)_2$ or oxo-acid/polymer blends such as BPEI/$0.5H_2SO_4$, the proton conductivity can be entirely explained by structure diffusion. In hydrated acidic polymers such as Nafion, proton conductivity is controlled by molecular diffusion. However, the boiling point of water limits the usage of water as a proton solvent at high temperature. H_3PO_4, due to the formation of 3D polyphosphoric acid network for proton transport at high temperatures and anhydrous environment, is the best solvent for proton

at high temperatures and anhydrous conditions. It has been demonstrated that in highly viscous anhydrous phosphoric acid, 98% of the total conductivity arises from structure diffusion of proton. Recently, Kreuer (Kreuer et al., 1998) proposed that imidazole (Fig. 3.3), benzimidazole and pyrazole could conduct proton as water does when ionized. After Kreuer's work, a series of work has been done with imidazole of benzimidazole as proton conductor (Ma Y., 2004).

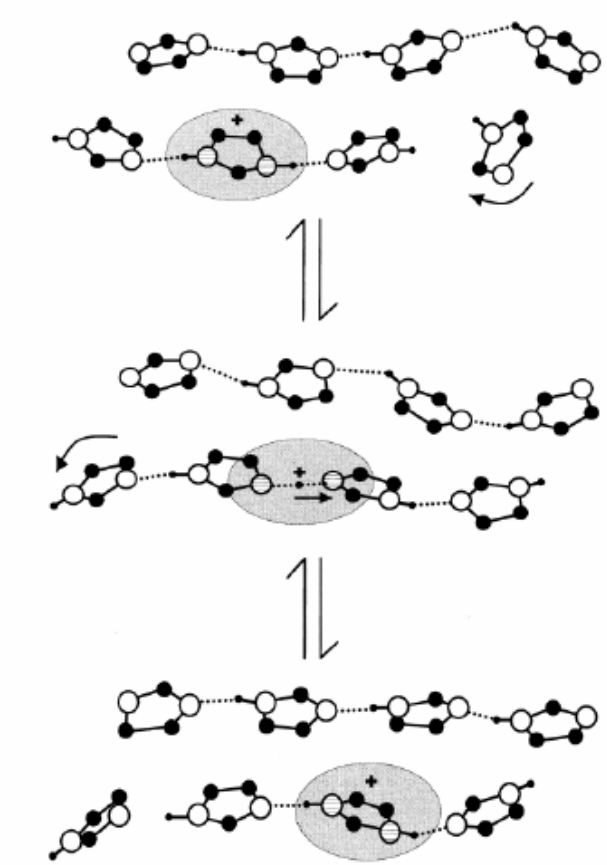

Figure 3.3. Proton conduction mechanism in liquid imidazole, as revealed by a Car-Parrinello molecular dynamics (CPMD) simulation (Kreuer et al., 2004).

Phosphoric acid, which can form 3-D hydrogen bonding network due to its special structure, is a very good proton conductive medium. The super-cooled melted pure acid has a conductivity of 0.053 S/cm at 30 ^{o}C, and this high value is known to come from the extensive self-ionization of H_3PO_4. Structure diffusion was proposed as the operating fast conduction and diffusion mechanism in fused phosphoric acid, where the transference number of proton is close to 1 (~0.975) (Dippel et al., 1993). Addition of

water increases the dissociation, decreases the viscosity therefore brings the conductivity to a maximum of 0.27 S/cm for 45% acid by weight (Chin and Chang, 1989). Further dilution decreases the number of charge carriers more rapidly than the viscosity, and the conductivity drops finally to the value of pure water. At high temperatures, phosphoric acid undergoes auto-dehydration process in addition to the self-dissociation process. The dehydration is reversible at low temperatures if water is provided. Therefore, phosphoric acid can conduct proton at high temperatures and very low relative humidity by forming polyphosphoric acid network.

It is well known that proton conducing polymer electrolyte can be obtained by doping polymers bearing basic groups such as ether, alcohol, imine, amide or imide with strong acids such as sulfuric acid. H_2SO_4 is more acidic and oxidative than H_3PO_4 and tends to form a salt with a basic site in the polymer thus decreases the concentration of the proton charge carrier. Moreover, the thermal stability of a H_2SO_4 doped polymer is not good due to its oxidizing property. H_3PO_4 is a relatively weak acid. It interacts with the polymer through hydrogen bond or proton transfer reaction depending on the basicity of the polymer. In acid/polymer systems, the polymer has two functions: on one hand, it has to be sufficiently basic to dissolve and complex with the acid, i.e. it acts as a solvent in which the acid undergoes some dissociation. On the other hand, excess acid is usually needed to obtain a high conductivity. Thus the polymer acts as a matrix to retain the excess acid. However, most of these materials suffer from fundamental limitations such as insufficient chemical stability (e.g. hydrolysis of esters or amides) or low mechanical stability, especially at higher temperatures or with excess acid. Films with good thermal and mechanical stabilities for high temperature application can be obtained from polymers with high glass transition temperatures such as polybenzimidazole. However, the segmental movement of polymer can assist the proton conductivity so that flexible polymers with low glass transition temperatures are preferred (Ma Y., 2004).

CHAPTER 4

POLYMER SYSTEMS

4.1 HYDRATED PROTON CONDUCTING MEMBRANES

In general, proton-conducting polymers are usually based on polymer electrolytes, which have negatively charged groups attached to the polymer backbone. These polymer electrolytes tend to be rather rigid and are poor proton conductors unless water is absorbed. The proton conductivity of hydrated polymer electrolytes dramatically increases with water content and reaches values of 10^{-2}-10^{-1} S cm^{-1}.

The first PEFC used in an operational system was the GE-built 1 kW Gemini power plant. This system was used as the primary power source for the Gemini spacecraft during the mid-1960s. The performances and lifetimes of the Gemini PEFCs were limited due to the degradation of poly(styrene sulfonic acid) membrane employed at that time. The degradation mechanism determined by GE was generally accepted until the present time. It was postulated that HO_2 radicals attack the polymer electrolyte membrane. The second GE PEFC unit was a 350 W module that powered the Biosatellite spacecraft in 1969. An improved Nafion membrane manufactured by DuPont was used as the electrolyte. Fig. 4.1 shows the chemical structures of Nafion and other perfluorinated electrolyte membranes. The performance and lifetime of PEFCs have significantly improved since Nafion was developed in 1968. Lifetimes of over 50,000 h have been achieved with commercial Nafion 120 (Rikukawa and Sanui, 2000).

.

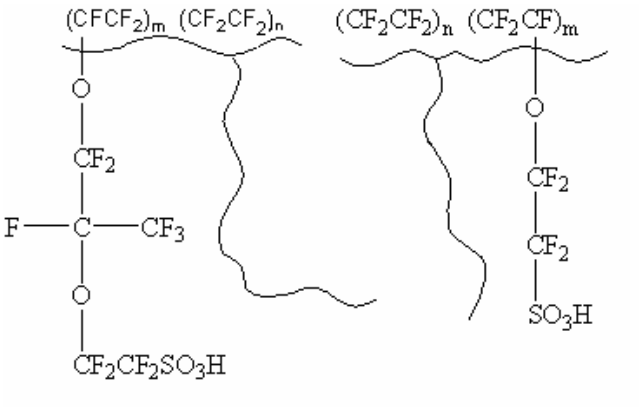

Figure 4.1. Chemical structures of perfluorinated polymer electrolyte membranes. (Sukumar, 2006).

According to Kreuer (Kreuer, 2001), perfluorosulfonic polymers have different microstructures from those of sulfonated aromatic polymers, as illustrated in Fig. 4.2. Nafion combines the extreme hydrophobicity of the perfluorinated polymer backbone with the extreme hydrophilicity of the terminal sulfonic acid function ($-SO_3H$). Especially in the presence of water, this gives rise to some amphiphilic nanoseparation. The sulfonic acid functional groups aggregate to form a hydrophilic domain. When this is hydrated, only the hydrophilic domain of the nanostructure is responsible for the transport of protons and water, while the hydrophobic domain provides the polymer with the morphological stability (mechanical strength) and prevents the polymer from dissolving in water. As a result, the water uptake by the Nafion membranes is very high (Sukumar, 2006).

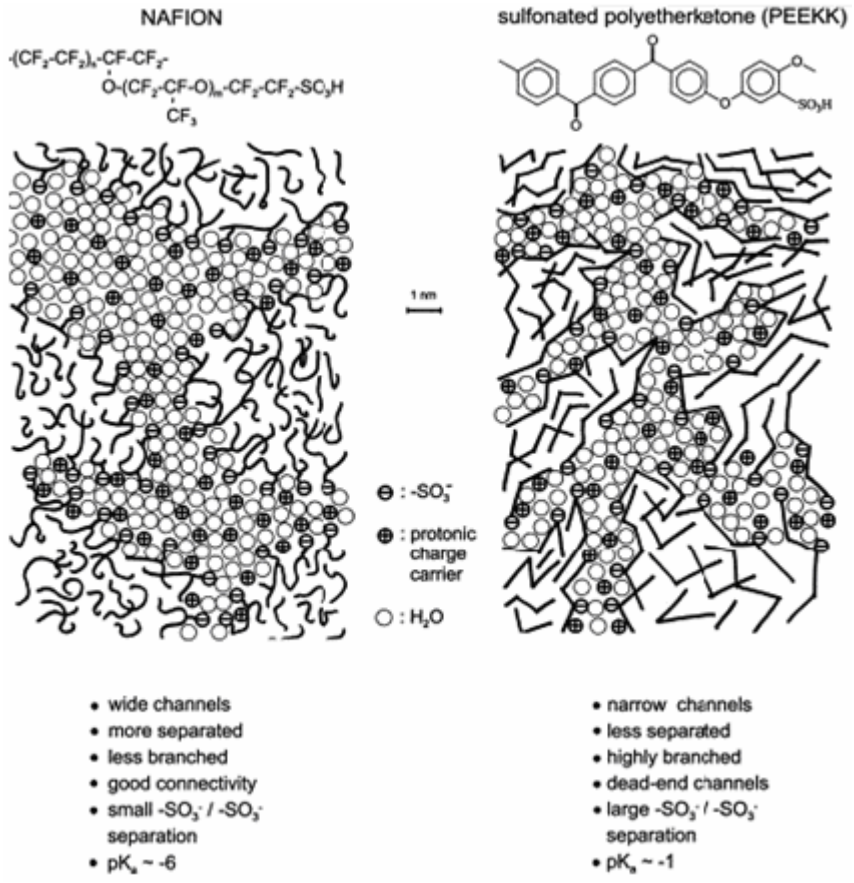

Figure 4.2. Schematic representation of the microstructures of Nafion and a sulfonated polyetherketone illustrating the less pronounced hydrophobic/hydrophilic separation of the latter compared to the first (Sukumar, 2006).

The situation in sulfonated aromatic polymers was found to be distinctly different with respect to both transport properties and morphological stability. In the case of sulfonated aromatic polymers, the hydrocarbon backbone is less hydrophobic and the sulfonic acid functional groups are less acidic and polar. As a result, the water molecules of hydration may be completely dispersed in the nanostructures of the sulfonated aromatic polymers (Rikukawa and Sanui, 2000). In general, PFSA and sulfonated aromatic polymers have similar water uptakes at low water activities, whereas at high relative humidity (100%), PFSA membranes have a much higher water uptake due to the more polar character of the sulfonic acid functional groups.

Consequently, the sulfonated polyaromatic membranes in general need more humidification during fuel cell operation in order to maintain the high level of conductivity. The less hydrophobic nature of the hydrocarbon nanostructure on the other hand may result in less dependence of conductivity on humidity in the low water activity range, allowing for good proton conductivity at high temperatures. For example, polyphenylenesulphide with a sulfonating degree of 200% exhibits a proton conductivity of the 10^{-2} S/cm level in the temperature range of 30-180 °C (Miyatake et al., 1997), whereas in Nafion membranes (Gavach and Pourcelly, 1992), the operating temperature is limited up to the boiling point of water.

4.2 ANHYDROUS PROTON CONDUCTIVE MEMBRANES

Basically, in anhydrous membranes, water is not necessary for proton conduction. Other molecules with high boiling point take the role of water as proton solvents in these membranes. Theoretically, any amphoteric molecule can do this job. However, not every amphoteric molecule exhibits high proton conductivity, especially in pure state. On the other hand, in contrast to using water as the proton solvent, which is usually supplied to the membrane by humidifying the anode and cathode gases and is produced at the cathode by the electrochemical reaction, the use of other proton solvents, such as phosphoric acid, sulfamide or heterocycle molecules, which can not be supplied during operation, requires their immobilization in the polymer membrane in such a way that high mobility of the protonic charge carriers is still guaranteed. The demand for proton conducting anhydrous membranes has been increasing over the last decade due to their use in fuel cells, as well as electrochromic displays, sensors and supercapacitors (Przyluski and Wieczorek, 1991; Lassegues, 1992; Lassegues et al., 2001; Schuster and Meyer, 2003).Although there are several approaches for anhydrous systems, previous concept was mainly based on the doping of the polymers bearing basic sites with protonic acids (e.g. H_3PO_4, H_2SO_4). Since pure H_3PO_4 themselves is a good proton conductor because of its extensive self-ionization and low pK_a. Structure diffusion was proposed as the proton diffusion mechanism in fused phosphoric acid, where the transference number of proton is close to unity (~0.975) (Dippel et al., 1993). Phosphoric acid interacts with polymers through hydrogen bonds depending on the basicity of the polymer and facilitates the formation homogeneous blends. In general,

phosphoric acid in polymer electrolytes acts as proton solvent via undergoing some dissociation and plasticizer where cooperative segmental motions of the polymer chains assist the proton diffusion. Several homogeneous polymer electrolytes such as poly(ethyleneoxide) $(H_3PO_4)_x$ (Donoso et al., 1988), poly(vinylalcohol) $(H_3PO_4)_x$ (Petty-Week et al., 1988), poly(acrylamide) $(H_3PO_4)_x$ (Rodriguez et al., 1993), poly(vinylpyrrolidone) $(H_3PO_4)_x$ (Bozkurt and Meyer, 2001) were reported. In addition, extensive research on more promising systems such as phosphoric acid doped polybenzimidazole, PBI have been focused on physicochemical characterizations as well as fuel cell applications (Schuster and Meyer, 2003; Samms et al., 1996; Li et al., 2003; Pu et al., 2002; Zhai et al., 2007).

4.2.1 Proton-Conducting Polymer Electrolyte Membranes Based on Acid-Base Polymer Complexes

There are different types of anhydrous proton conducting acid-base membranes reported in literature, with a focus on PBI/H_3PO_4 (Wainrigh et al., 1994) blends that are currently most suitable for fuel cell applications. In acid-base membranes, the property of the acid (H_3PO_4 or H_2SO_4) to interact via hydrogen bonds facilitates the preparation of blends with a variety of polymers, such as PBI (Wainrigh et al., 1994), poly(4-vinylimidazole) (Bozkurt and Meyer, 2001a), polyethyleneoxide (Donoso et al.,1988), and poly(vinylpyrrolidon) (Bozkurt and Meyer, 2001b). Proton conduction in acid-base membranes is strongly dependent on the nature of acid (Chin and Chang, 1989; Dippel et al., 1993; Kreuer, 2000; Pu et al., 2002; Bouchet and Siebert, 1999), polymer (Hickman et al., 1999; Hoel and Grunwald, 1977), temperature (Pu et al., 2001; Bozkurt and Meyer, 2000) and humidity (Pu, 2003).

Phosphoric acid is a weak acid ($pK_a = 2.16$) (Lide, 1995) that melts at 42 °C in the pure state and acts as an oxidant at elevated temperatures. With basic polymers, phosphoric acid undergoes hydrogen bond interactions or proton transfer reactions. In regard to its conductivity, phosphoric acid differs from water and many other solvents in two ways. First, conductivity is remarkably high in the pure state (Chin and Chang, 1989). Second, when strong electrolytes (e.g., H_2SO_4) are added, conductivity decreases rather than being improved (Munson and Lazarus, 1967). The first feature is due to the

generation of charge carriers by self-dissociation ($5H_3PO_4 = 2H_4PO_4^+ + H_2PO_4^- + H_3O^+ + H_2P_2O_7^{2-}$, where H_3PO_4 = 16.8 M, $H_4PO_4^+$ = 0.89 M, $H_2PO_4^-$ = 0.43 M, H_3O^+ = $H_2P_2O_7^{2-}$ = 0.46 M at 311 K) and the fact that proton migration almost entirely results from structure diffusion (Dippel and Kreuer, 1993). The second feature is also closely related to the transport mechanism. The electrical field of extrinsic charge carriers causes a bias on hydrogen bonds and thus suppresses fluctuations within the dynamical hydrogen bond network (Kreuer, 1996; Kreuer, 2000). Addition of water, however, increases conductivity, which passes through a temperature-dependent maximum at compositions of 45 to 60% of H_3PO_4 (Chin and Chang, 1989).

4.2.1.1 Boronic Acid

4.2.1.1.1 Structure and Properties of Boronic acid

Structurally, boronic acids are trivalent boron-containing organic compounds that possess one alkyl substituent (i.e., a C–B bond) and two hydroxyl groups to fill the remaining valences on the boron atom (Fig. 4.3). With only six valence electrons and a consequent deficiency of two electrons, the sp^2-hybridized boron atom possesses a vacant p orbital. This low-energy orbital is orthogonal to the three substituents, which

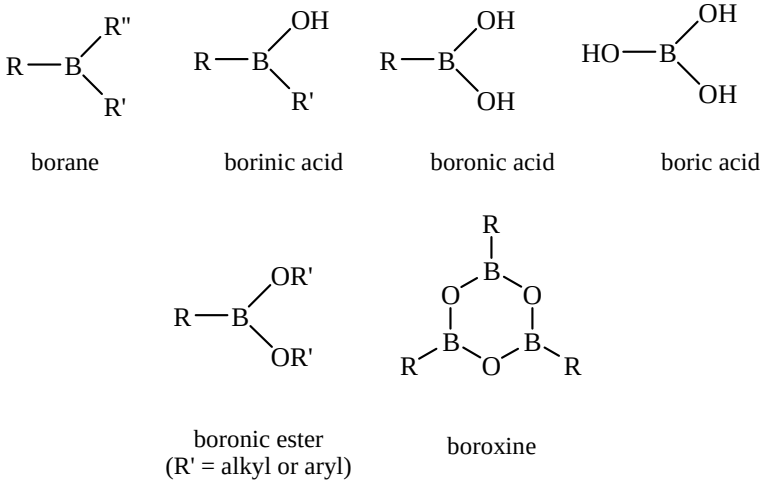

Figure 4.3. Boron compounds (Hall D.G., 2005).

are oriented in a trigonal planar geometry. Unlike carboxylic acids, their carbon analogues, boronic acids are not found in nature.

These abiotic compounds are derived synthetically from primary sources of boron such as boric acid, which is made by the acidification of borax with carbon dioxide. Borate esters, the main precursors for boronic acid derivatives, are made by simple dehydration of boric acid with alcohols. The first preparation and isolation of a boronic acid was reported by Frankland in 1860 (Frankland and Duppa, 1860).

The reactivity and properties of boronic acids is highly dependent upon the nature of their single variable substituent; more specifically, by the type of carbon group (R) directly bonded to boron. In the same customary way as for other functional groups, boronic acids are classified conveniently in subtypes such as alkyl-, alkenyl-, alkynyl-, and aryl- boronic acids.

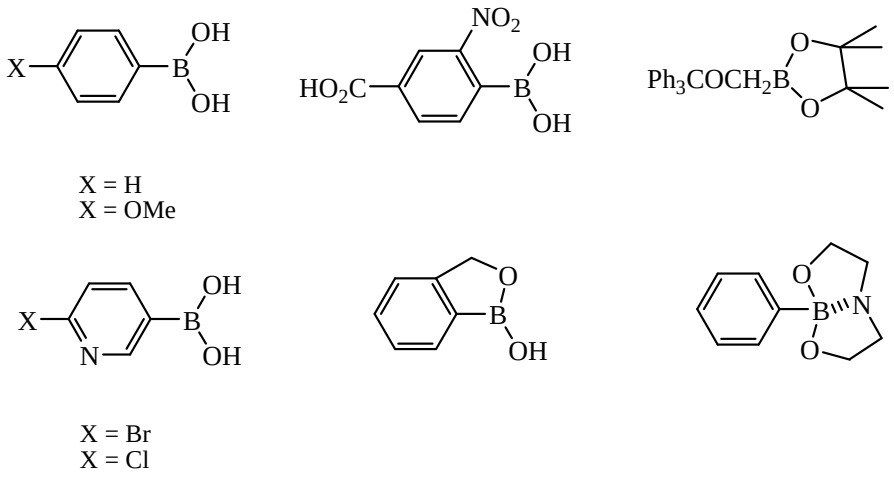

Figure 4.4. Boronic acid derivatives analyzed by X-ray crystallography (Hall D.G., 2005).

Most boronic acids exist as white crystalline solids that can be handled in air without special precautions. At ambient temperature, boronic acids are chemically stable and most display shelf-stability for long periods. The X-ray crystal structure of phenylboronic acid (Fig. 4.4) was reported in 1977 by Rettig and Trotter (Rettig and Trotter, 1977).

The crystals are orthorhombic, and each asymmetric unit consists of two distinct molecules, bound through a pair of O–H---O hydrogen bonds (A and B, Fig. 4.5). The CBO_2 plane is quite coplanar with the benzene ring, with a respective twist around the C–B bond of 6.6° and 21.4° for the two independent molecules of $PhB(OH)_2$. Each dimeric ensemble is also linked with hydrogen bonds to four other similar units to give an infinite array of layers (C, Fig. 4.5).

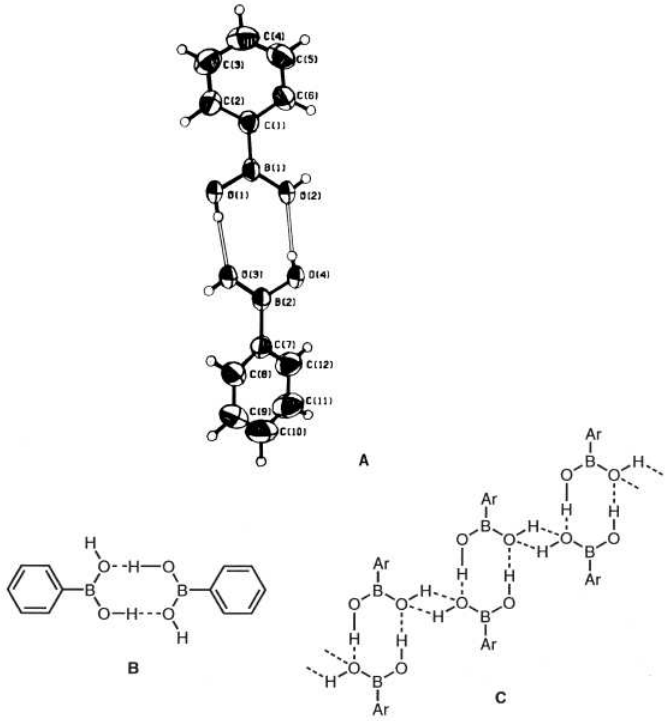

Figure 4.5. Representations of the X-ray crystallographic structure of phenylboronic acid. (A) ORTEP view of a dimeric unit. (B) Dimeric unit showing hydrogen bonds. (C) Extended hydrogen-bonded network (Hall D.G., 2005).

4.2.1.1.2 Important Application of The Boronic Acid Carrying Materials

The reversible complex formation between phenylboronic acid and diol carrying molecules was extensively investigated by different researchers (Yamamato et al., 1998; Tong et al., 2001; Springsteen and Wang, 2002; Cabell et al., 1999). Among the different oxidation states, boronic acid is the most useful for biological application because of (1) its ready inter-convertibility between the $sp^2$and sp^3 forms, (2) its strong

interaction with diol-containing compounds (Fig. 4.6), (3) its lewis acidity, and (4) is unique behaviour upon neutron bombardment (Hall D.G., 2005).

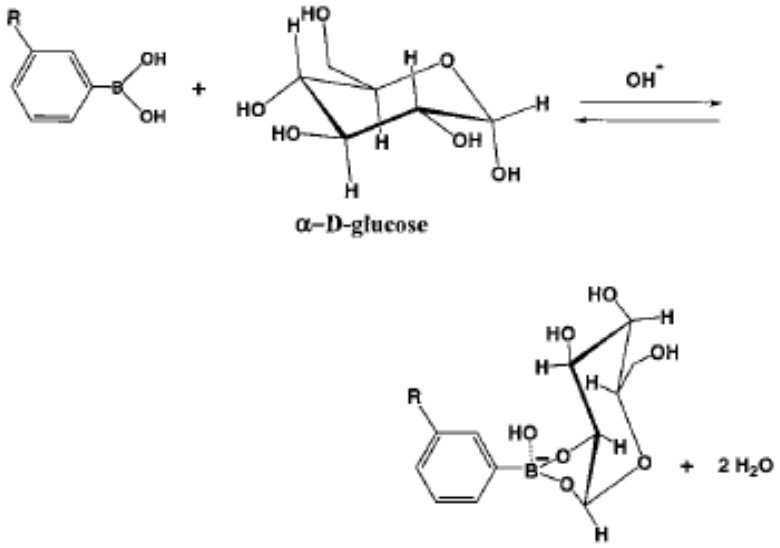

Figure 4.6. Equilibrium for the boronic acid/diol (sugar) and OH^- interaction (Gabai et al., 2001).

Based on this interaction, phenylboronic acid functionalized polymers were used as carriers in the chromatographic studies involving the separation of diol carrying biomolecules like sugars, nucleotides, nucleic acids, enzymes and glycoproteins (Koyama and Terauchi, 1996; Uguzdogan et al., 2002 ; Elmas et al., 2004; Tuncel and Ozdemir, 2000; Camli et al., 2002) or in drug delivery (Shiino et al., 1995) and specific detection (Gao et al., 2001; Appleton and Gibson, 2000). Another important application of the boronic acid carrying materials is the development of fluorescent sensors for diol detection. Fluorescent probes based on free or immobilized phenylboronic acid were synthesized particularly for the recognition of carbohydrates (Kitano et al., 1998; Adhikiri et al., 1999; James et al., 1995; Oguzdogan et al., 2003; Gardiner et al., 1999). A reusable optical nanosensors for carbohydrate recognition was developed based on boronic acid functionalized poly(chloromethylstyrene) latex particles (Canizzo et al., 2005). A temperature-sensitive copolymer of 2-dimethylacrylamide and 3-acrylamidophenyl-boronic acid (AcPBA) was synthesized by solution polymerization (Kataoka et al., 1994). The linear copolymers of N-isopropylacrylamide (NIPA) and AcPBA and the terpolymer of NIPA-AcPBA-dimethylaminopropylacrylamide

(DMAPA) exhibited a lower critical solution temperature (LCST) shift against carbohydraten concentration (Aoki et al., 1996; Hisamitsu et al., 1997; Shiomori et al., 2004).

4.2.1.2 Nitrogen-Containing Aromatic Heterocycles as Proton Carriers

Historically, the interest in hydrogen bonding and proton conductivity in heterocycles has its roots in speculations about the participation of hydrogen bonds in energy and charge transfer in biological systems (Kawada et al., 1970); specifically, concerning the participation of NH----N bonds between the imidazole groups of histidine in proton transport in transmembrane proteins (Decoursey, 2003). Even Zundel has worked in the field (Zundel and Weidemann, 1971), and it is not surprising that his view of the proton dynamics in imidazole is closely related to that of water.

However, the conductivity of liquid imidazole is several orders of magnitude higher (~10^{-3} S/cm at the melting point of T_m = 90 °C) (Kawada et al., 1970); however, its mechanism was investigated much later. It was the search for chemical environments that were different from water in fuel cell membranes that brought heterocycles back into focus. The potential proton donor and acceptor functions (amphoteric character), the low barrier hydrogen bonding between the highly polarizable N atoms, and the size and shape of the molecule were reasons that Kreuer started to investigate the usefulness of heterocycles as proton solvents in separator materials for fuel cells. This work also comprises the study of the transport properties of neat and acidified liquid imidazole, pyrazole, and, later, benzimidazole (Kreuer et al., 1998).

The region containing the excess proton (intentionally introduced) is an imidazole with both nitrogens protonated and acting as proton donors toward the two next nearest imidazoles in a configuration Imi---ImiH^+---Imi with hydrogen bonds (~273 pm) slightly contracted, compared to the average bond length of the system, but still longer than the bonds in the isolated complex (in the gas phase) (Tatara et al., 2003). The position of the protons within these hydrogen bonds is dependent mainly on the hydrogen bonding between the nearest and next-nearest solvating imidazoles.

The hydrogen-bonded structure in imidazole is observed to be chainlike (i.e., low dimensional), with two possible orientations of the hydrogenbond polarization within segments which are separated by imidazoles with their protonated nitrogen directed out of the chain. This may even form a “cross-linking” hydrogen bond with a nonprotonated nitrogen of a neighboring strand of imidazole. The simulation data revealed the existence of imidazole molecules close to the protonic defect in hydrogenbond patterns, which rapidly change by bond breaking and forming processes. Similar to water, this shifts the excess proton within the region and may even lead to complete proton transfer (Kreuer et al., 2004). There is no indication of the stabilization of a symmetrical complex $(Imi\text{---}H\text{---}Imi)^{+}$: there always seems to be some remaining barrier in the hydrogen bonds, with the proton being on one side or the other. As illustrated for the most simple mechanism of this type in Fig. 4.7, the sum of all proton

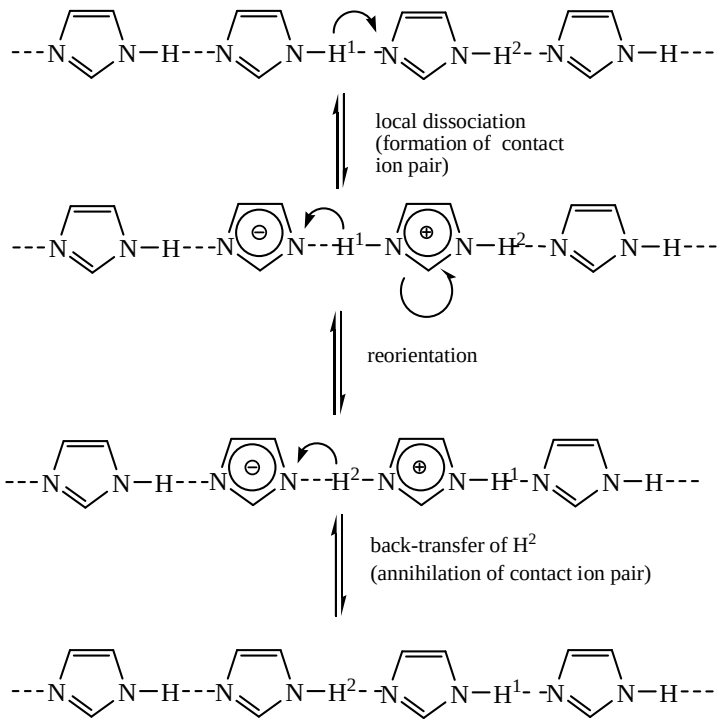

Figure 4.7. Schematic illustration of correlated proton transfers in pure liquid imidazole leading to proton diffusion but not proton conductivity (Kreuer et al., 2004).

translocation vectors form a closed trajectory reminiscent of cyclic intermolecular proton-transfer reactions known to occur in certain organic pyrazole-containing complexes (Toda et al., 1993) and proton diffusion in hydroxides (Spaeth et al., 1997; Spaeth et al., 1999).

The self-dissociation constants for heterocycles (in particular, imidazole) are actually much higher than for water, but degrees of self-dissociation (concentration of protonic charge carriers) of ~10^{-3} are still ~2 orders of magnitude lower than that for phosphoric acid (Kreuer et al., 2004).

4.2.1.3 Heterocycle Molecules and Phosphoric Acid as Proton Solvent in Polymeric Mixtures

4.2.1.3.1 *P4-VIm/H_3PO_4*

Meyer et al. (Bozkurt and Meyer, 2001a; Pu et al., 2001) synthesized poly (4-vinyl-imidazole) (P4-VIm), where the imidazole is directly bonded to the backbone. The conductivity of pure P4-VIm is comparatively low (2 x 10^{-10} S/cm at 150 ^{o}C) (Bozkurt and Meyer, 2001a). Reasonable conductivities are only obtained in the blends with H_3PO_4 or H_2SO_4 (10^{-3} S/cm for x = 1 at ambient temperature) (Pu et al., 2001). The conductivity increases with x for H_3PO_4 and reaches similar to 10^{-4} S/cm for x = 2 at ambient temperature. The blend is thermally stable up about 150 ^{o}C.

4.2.1.3.2 *PBI/H_3PO_4*

Savadogo compared the conductivity of PBI membranes doped in various acids, and found that the conductivity changes are in the order of H_2SO_4 > H_3PO_4 > $HClO_4$ > HNO_3 > HCl for high doping levels (Xing et al., 1995). Moreover, they studied alkaline-doped PBI (KOH, NaOH, and LiOH) (Xing et al., 2000). The highest conductivity of KOH-doped PBI (Xing et al., 2000) (9 x 10^{-2} S/cm, doped in 6 M KOH, measured in doping solution at 60 °C) is higher than those of sulphuric acid-doped PBI (6 x 10^{-2} S/cm, doped in 16 M H_2SO_4 solution and measured in 2 M $HClO_4$ solution at

25 °C) and H_3PO_4 doped PBI (2 x 10^{-3} S/cm, doped in 15 M H_3PO_4 solution and measured in 2 M $HClO_4$ solution at 25 °C) (Xing et al., 1995). Staiti studied the conductivity of PBI membranes mixed with phosphotungstic acid (PWA) adsorbed on SiO_2, and obtained 1.5 x 10^{-3} S/cm at 90-150 °C (Slaiti et al., 2000). They also studied sulfonated PBI and obtained high thermal stability but low proton conductivity (7.5 x 10^{-5} S/cm at 100% RH and 160 °C) (Slaiti et al., 2001). They attributed this result to strong interaction between protons and nitrogen atoms of the imidazolium ring in PBI, which reduces the proton mobility, producing a slightly semicrystalline polymer. Akita casted PBI membranes doped with aromatic phosphoric acid monoand di-esters (i.e., at least one hydrogen atom of phosphoric acid is substituted by a molecule containing a phenyl group) in order to prevent the acid dopants from being leached out by water (Akita et al., 2000). They obtained conductivity up to 5 x 10^{-3} S/cm in a dried state at 200% diphenyl phosphoric acid doped PBI at 125 °C (Sukumar, 2006).

4.2.1.3.3 *Poly(VPA-co-4-VIm)*

Copolymers of vinylphosphonic acid and 4-vinylimidazole are reported (Bozkurt et al., 2003). The copolymers are thermally stable at least up to 200 °C. The DC conductivities of the dry copolymers are between 10^{-6} and 10^{-12} S/cm within the measured temperature regime. The DC conductivities increase with increasing imidazole units which are immobilized in the chains.

4.2.1.3.4 *PAMPSA–xIm blends*

Blends of poly(2-acrylamido-2-methyl-1-propanesulfonic acid) (PAMPSA) with imidazol (Imi) are reported (Erdemi et al., 2002). These blends can be cast into homogeneous films. DSC shows that the softening temperature of the blends decreases from 87 ºC for x = 0.5 to -25 ºC for x = 2. PAMPSA–xImi blends are thermally stable up to 180 ºC. With increasing Imi content the glass transition temperature of the pristine polymer decreases while the conductivity of the blends increase with x, reaching 10^{-3} S/cm at 100 ºC. The proton migration may occur through movement of the proton vacancies that is a Grotthuss type diffusion mechanism.

4.2.1.3.5 *Adipic Acid/Benzimidazole Electrolytes*

Karadedeli et al. investigated several blends of a diacid, adibic acid (AA) and heterocycle base, benzimidazole (BIm). Thermogravimetry analyses indicate that these materials are thermally stable up to 160 °C. Adipic acid has very low proton conducivity (~10^{-11}) in crystaline form. The conductivity of the blends increased with BIm and reached a maximum conductivity of 4 x 10^{-3} S/cm at 130 °C.

4.2.1.3.6 *PAAxIm Blends*

Anhydrous proton conducting polymer electrolytes have been prepared by entrapping Imi in polyacrylic acid (PAA) (Bozkurt et al., 2003). These blends were thermally stable to about 160 ^{o}C. The initial weight loss above 160 ^{o}C for x = 1 was attributed to evaporation of dopant and followed decomposition of the blends above 200 ^{o}C. The conductivity increases with x and temperature, reaching ~10^{-3} S/cm for x = 1 at 120 ^{o}C. For x larger than 1, phase separation appears. FT-IR spectra showed the transfer of the acidic proton of the carboxylic acid to the “free” nitrogen side of imidazole to form imidazolium ion. The proton migration might occur through a Grotthuss type mechanism. From the sdc isotherm, it was concluded that the proton transport was controlled by the segmental motions of the polymer chains.

4.2.1.3.7 *Nafion/* H_3P0_4 *, Nafion/Triazole and Nafion/Benzimidazole Composite*

Savinell et al. studied Nafion/H_3P0_4 that has been evaluated with respect to water content, ionic conductivity and transport of oxygen, and methanol vapor. The results show that at elevated temperatures reasonably high conductivity can be obtained. Methanol permeability is shown to be proportional to the methanol vapor activity and thus decreases with increasing temperature for a given methanol partial pressure.

Anhydrous proton-conducting polymers employing Nafion–1,2,4-triazole- and Nafion–benzimidazole-blend membranes were studied for use in PEFCs above 100 °C. The solvents 1,2,4-triazole and benzimidazole are thermally stable, organic reagents

with low volatility and are used to replace water as the proton acceptor in the perfluorinated ionomer membrane. The Nafion–benzimidazole blend had high thermal stability above 200 °C . The conductivity of the membranes with n = 14.5 (n is defined as the ratio of 1,2,4-triazole to $–SO_3H$ in Nafion–1,2,4-triazole) and with n = 8.5 (n is defined as the ratio of BIm to $–SO_3H$ in Nafion–BIm) reached 2.3 x 10^{-2} S/cm at 160 °C and 8.64 x 10^{-3} S/cm at 200 °C, respectively (Kim et al., 2007).

CHAPTER 5

EXPERIMENTAL

5.1 SYNTHESIS OF POLYMERS

5.1.1 Materials and Preparation

4-Vinylbenzeneboronic acid (VBBA) (98%) was kindly provided by Alfa Aesar (Johnson Matthey Company). α,α'– Azodiisobutyramidin Dihydrochlorid purum (AIBADC) initiator (98%) were supplied from Aldrich. Urocanic acid (UA) were supplied from Sigma**.** Orthophosphoric acid (99%) and N,N-Dimethylformamide (DMF) were purchased from Merck and they are all reagent grade and were used as received. Glycidyl methacrylate (GMA) (Fluka), initiator 2,2'-azobisisobutyronitrile (AIBN) (Fluka), ethanol amine (Merck), boric acid (Fluka) and other chemicals are reagent grade and used without further purification.

5.1.2 Synthesis of Homopolymer PVBBA

Poly(4-vinylbenzeneboronic acid), PVBBA was produced by free radical polymerization of VBBA in DMF using AIBADC as initiator. The reaction mixture was purged with nitrogen and the polymerization reaction was performed at 80 ºC for 4 h (Fig. 5.1). After polymerization of VBBA in DMF, the resulting solid was filtered and washed with excess DMF. The gelly material was cast onto polished PTFE plates. After drying under vacuum, transparent and insoluble films were obtained.

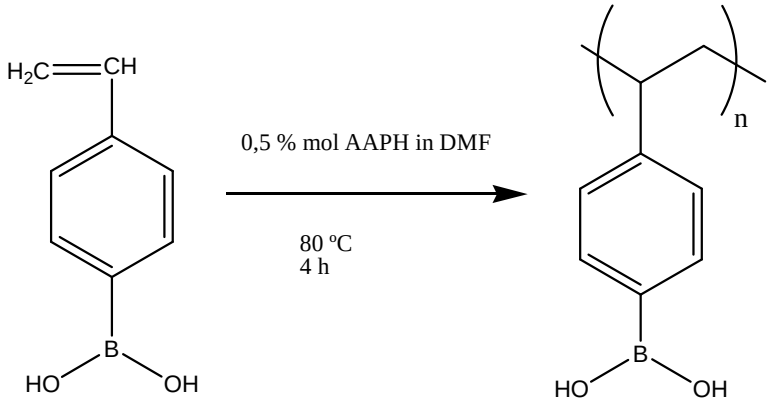

4-VBBA PVBBA

Figure 5.1. Synthesis scheme of PVBBA.

5.1.3 Synthesis of 4-Vinylimidazole Monomer

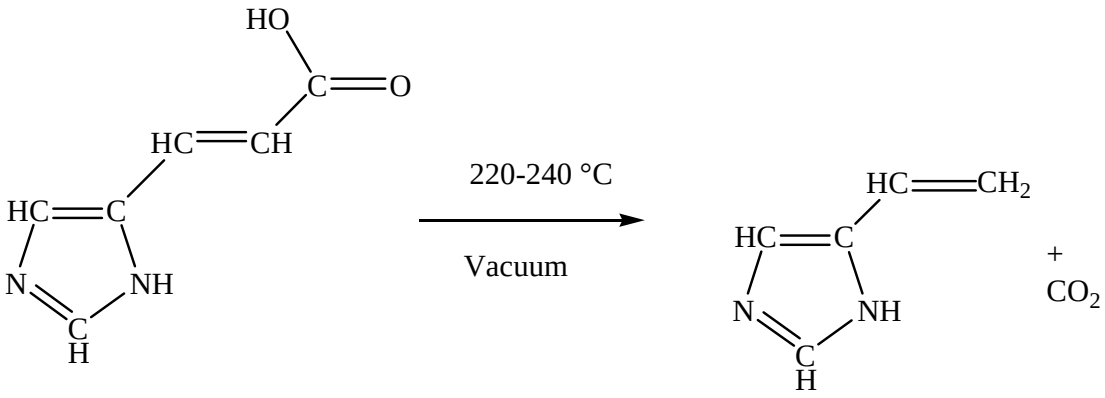

Uroconic acid 4-Vinylimidazole

Figure 5.2. The synthesis of 4-vinylimidazole.

4-VIm was synthesized as described in the literature (Overberger and Vorchheimer, 1963). Anhydrous urocanic acid (UA) was heated under the vacuum. At a temperature of 220 °C, the material melted and began to decompose at 240 °C, as noticed by a decreased vacuum (Fig. 5.2 and Fig. 5.3). At a temperature of 220 °C, UA starts undergoing decarboxylation to generate the desired 4-vinylimidazole.

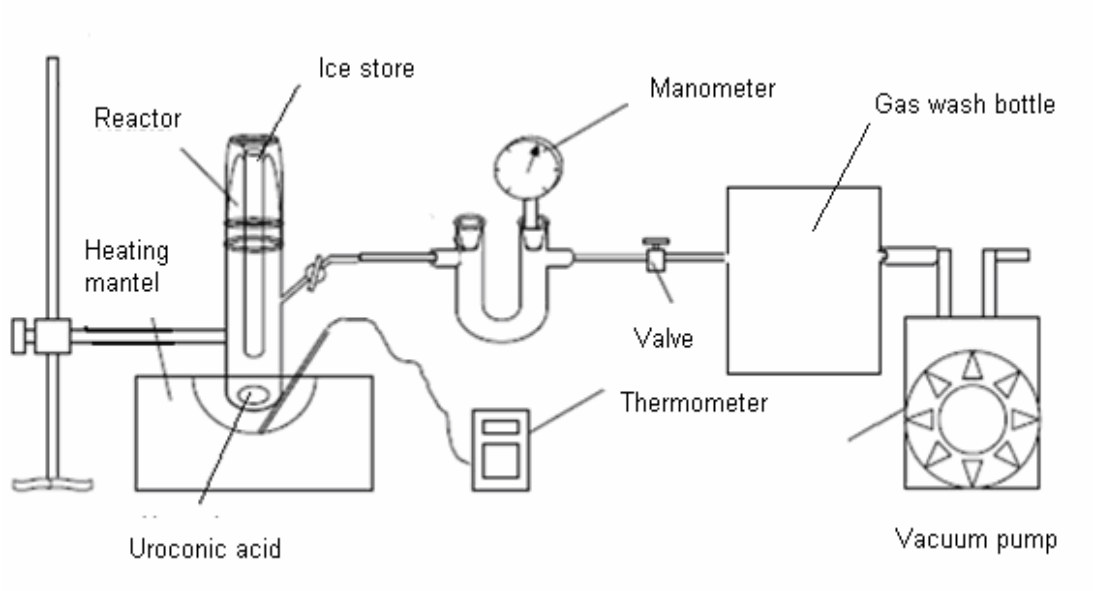

Figure 5.3. Reactor for Monomer Synthesis.

UA was melted and then decomposed near 240 °C to generate the desired monomer which is crystallized on a cold receiver as pale yellowish solid (yield: ~40%). The low yield is in part due to thermal decomposition of the starting material at this temperature to give an insoluble black material.

5.1.4 Synthesis of Poly(4-VBBA-co-4-VIm) Copolymers

The copolymer were synthesized by free-radical polymerization of 4-VIm and VBBA at various monomer feed ratio as compiled in Tablo 5.1. DMF and AIBN were used as the polymerization solvent and initiator, respectively. The copolymer S1 (1:1 feed mol ratio) was synthesized by dissolving 0,46g 4-VIm and 0,72g VBBA in DMF at 80 °C, using AIBN as initiator. The initiator concentration was 1,5% with respect to total number of moles of monomers. The reaction mixture was homogenized polymerizations were conducted under nitrogen atmosphere. After polymerization the copolymers, poly(4-VBBA-co-4-VIm), which was precipitated form the solution as yellowish solid, was filtered and washed with excess DMF to remove unreacted monomer.

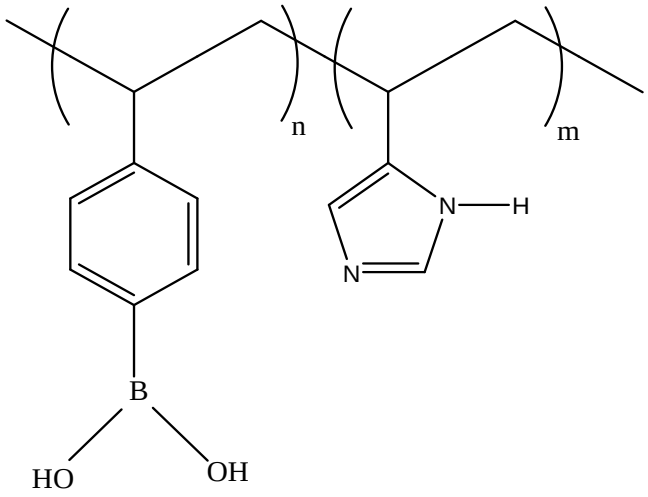

Figure 5.4. Molecular structure of poly(4-VBBA-co-4-VIm) copolymer

The products were dried under vacuum at 60 °C for several days. Copolymers (Fig. 5.4) were obtained as powder which was insoluble in common organic solvents and aqueous medium The actual compositions of the copolymers, whichwere calculated from the elemental analysis data are summarized in Table 5.1. The composition of the copolymer is only slightly depending on the monomer feed ratio. When 4-VIm in the feed ratio is varied from 25% to 66%, the 4-VIm content in the copolymer is changed from 36% to 65%.

Table 5.1. 4-VIm contents of Poly(4-VBBA-co-4-VIm) calculated by Elemental Analysis results

Sample	Feed ratio(mol) 4-VIm : 4-VBBA	AIBN*10^{-3}(mol)	Yield (%)	N (%)	4-VIm (%)
S1	1:1	9,92	84	11,35	49,2
S2	1:2	5,57	87	8,89	40,1
S3	1:3	4,74	44	8,00	36,6
S4	2:1	4,45	64	11,56	50.0

5.1.5 Synthesis of Boric Acid Functional Polyacrylate

5.1.5.1 Synthesis of PGMAN

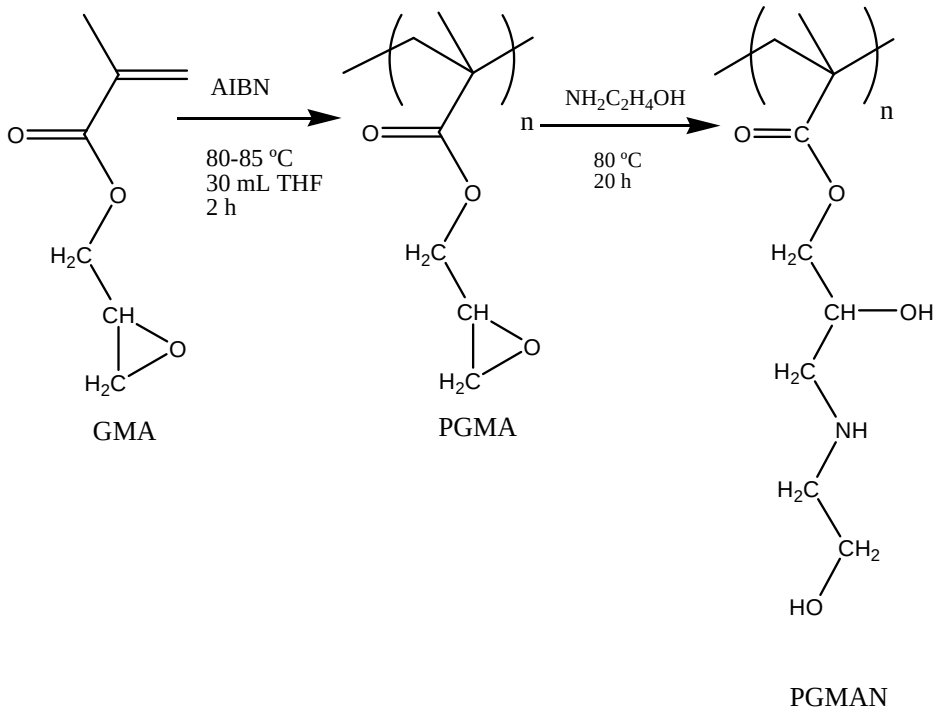

Figure 5.5. Synthetic route of PGMAN polymer.

A three-necked flask was equipped with a mechanical stirrer, nitrogen inlet and reflux condenser. To the falsk 0,52g GMA and (1% mol ratio) AIBN in 30 ml THF was added, while stirring stirring nitrogen was purged through the mixture. After stirring for 2 h at 80-85 ºC, 1,12g ethanolamine was added to the mixture and refluxed for 20 h. The PGMAN polymer was collected by filtration, washed with deionized water and dried under vacuum at 60 ºC for 2 h (Fig. 5.5).

5.1.5.2 Synthesis of Borate-Loaded Polymers (PGMANB)

The synthesis of PGMANB was started with the radical polymerization of GMA with the initiation of AIBN and followed functionalization of PGMA by ring-opening reaction of oxirane with amine groups of ethanolamine to yield hydroxyl functionalized PGMAN (Fig. 5.5). The PGMAN polymer was further reacted with boric acid in a molar ratio of 1:1. The PGMANB complex was obtained after the mixture was shaken at room temperature for 72 h, filtered, washed and dried under vacuum at 60 ºC for 2 h (Fig. 5.6).

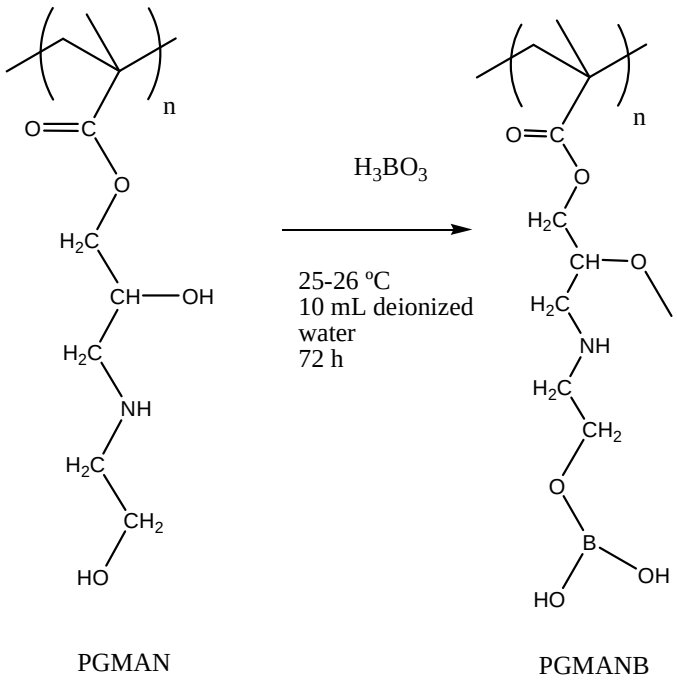

PGMAN PGMANB

Figure 5.6. Synthesis of PGMANB.

The functionalization of the polymer was successfully proven by the elemental analysis and the hydroxyl group contents of the samples were calculated through nitrogen analysis. The results are summarized in Table 5.2. It is obvious that the hydroxyl groups are at least 84% accessible to epoxy ring of PGMAN.

Tablo 5.2. Elemental Analysis of PGMAN

%C	%H	%N
49,87	8,08	6,11

5.2 Synthesis of Doped Samples

5.2.1 Synthesis of H_3PO_4 Doped PVBBA

Doping of the polymers was performed at different stoichiometric ratios, x by swelling of the polymer in concentrated solution of phosphoric acid in DMF and the solution was stirred 2 days at room temperature in the glow box. Solution with x = 1 and x = 2 (mol ratios) were prepared where x is the molar ratio of acid to benzeneboronic acid unit that has already been polymerized. The swelled gels were spread over polished PTFE plates and the solvent was evaporated under nitrogen atmosphere. The materials were further dried under vacuum (at 50 °C for several days, until constant weight was reached). Transparent and homogeneous and thin film of PVBBAH_3PO_4 and PVBBA$(H_3PO_4)_2$ were obtained.

5.2.2 Synthesis of H_3PO_4 Doped Poly(4-VBBA-co-4-VIm)

Polymer electrolytes were prepared by swelling of the copolymer S1 in phosphoric acid/DMF solution. Stoichiometric amounts copolymer and phosphoric acid were admixed in DMF and the solution was stirred 48 hour at room temperature in the glow box. Solution with x = 1 and x = 2 (mol ratios) were prepared where x is the molar ratio of acid to imidazole that has already been immobilized in the polymer chain. The swelled gels were spread over polished PTFE plates and the solvent was evaporated under nitrogen atmosphere. The materials were further dried under vacuum (at 50 °C for 3 days, until constant weight was reached). Transparent and homogeneous and thin film of poly(4-VBBA-co-4-VIm)H_3PO_4 and poly(4-VBBA-co-4-VIm)$(H_3PO_4)_2$ were prepared.

5.3 Characterizations

Fourier-Transform IR spectra of the samples were scanned using a Mattson Genesis II spectrophotometer. Solid ^{13}C NMR and ^{11}B MAS-NMR study of the phosphoric acid doped copolymer was performed using a 700 MHz Bruker Avance spectrometer in the Max-Planck Institute for Polymer Research, Mainz, Germany. The composition of nitrogen in the copolymers was measured by elemental analysis using LECO, CHNS-932 instrument at METU, Ankara. The imidazole content of the copolymer was evaluated through percent nitrogen analysis. The structure features of the copolymer samples were recorded by X-ray powder diffractometry (XRD). Thermal stabilities of the copolymer electrolytes were examined by TG analyses with a Perkin Elmer Pyris 1. The samples (~10 mg) were heated from room temperature to 800 ^{o}C under N_2 atmosphere at a scanning rate of 10 ^{o}C/min. DSC measurements were carried out on a Netzsch Differential Scanning Calorimeter DSC 404 C Pegasus under nitrogen atmosphere and heating-cooling curves were recorded at a rate of 10 ^{o}C/min. The proton conductivity studies of the samples were performed using a SI 1260-Schlumberger impedance spectrometer in the Max-Planck Institute for Polymer Research, Mainz, Germany. The conductivities were measured in the frequency range 0.1 Hz to 1 MHz at 10 ^{o}C intervals. The DC conductivities of the samples were derived from the AC conductivity data.

CHAPTER 6

CHARACTERIZATION OF PROTON CONDUCTING POLYMER ELECTROLYTES

6.1 FT-IR STUDIES

6.1.1 FT-IR of Poly(4-Vinylbenzeneboronic acid) and H_3PO_4 Doped Samples

The IR spectra of homopolymer PVBBA and acid doped PVBBA$(H_3PO_4)_2$ are shown in Fig. 6.1. The OH stretching of $-B(OH)_2$ group gives a broad peak at around 3380 cm^{-1}. The aromatic CH stretching was at 3030 cm^{-1} , the absorption bands at 2930 and 2850 cm^{-1} were assigned to the symmetric and antisymmetric stretching

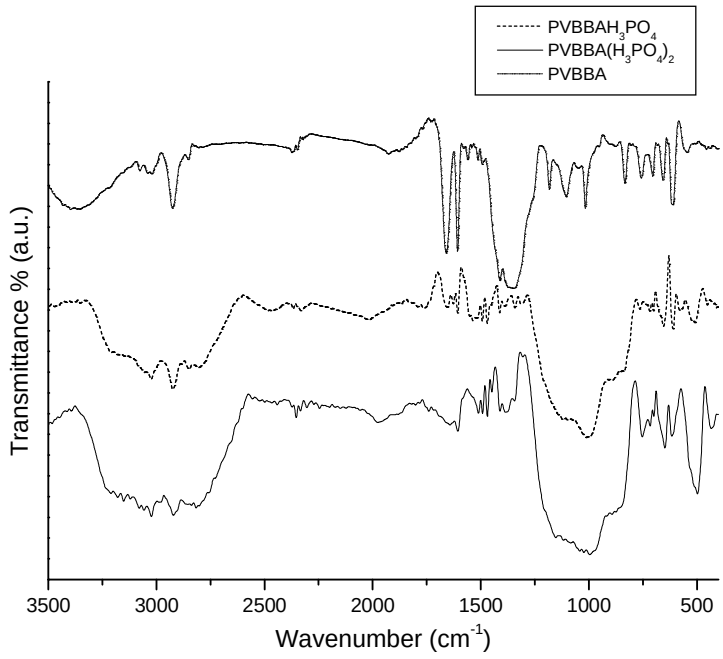

Figure 6.1. FT-IR spectra of PVBBA and doped samples.

vibration of aliphatic CH units. The strong peak at 1606 cm^{-1} is attributed to C=C stretching in phenyl ring. The vibration of phenyl boronic acid linkage (Ph–B) gives a strong peak at 1470-1410 cm^{-1}. The absorption bands at 1342 and 1105 cm^{-1} were assigned to the vibration of the bond B–O and B–OH . The OH deformation in $–B(OH)_2$ was at 1006 cm^{-1} (Kahraman et al., 2004). The strong CH out-of plane deformation band for p-disubstituted benzene ring was at 835 cm^{-1}. Other important absorption signal near 760 cm^{-1} corresponds to B-O-B stretching vibration due to the cross-linked (Bozkurt et al., 2005). The absorption bands at 655 and 615 cm^{-1} were assigned to out of plane OH bending with stronger H-bond (Kahraman et al., 2004).

After doping the PVBBA with H_3PO_4, two strong peaks appear near 500 cm^{-1} and 1000 cm^{-1} which are attributed to PO_2 bending vibration and P-OH symmetric stretching of H_3PO_4 . The broad band between 2500-3000 cm^{-1} is attributed to the P-OH bending of the phosphoric acid (Bouchet et al., 1999). The intensity of the peaks that correspond to $B-(OH)_2$ and B-OB bonds decreased for x = 1 $PVBBAH_3PO_4$ which may be due to the masking effect of phosphoric acid.

6.1.2 FT-IR of poly(4-VBBA-co-4-VIm) Copolymers and H_3PO_4 Doped Samples

The FT-IR specra of poly(4-VBBA-co-4-VIm) copolymers (S1, S2, S3 and S4) are represented in Fig. 6.2. The five-membered heteroaromatic rings exhibit a strong absorption at 800-700 cm^{-1}, which can be related to C-H out-of-plane vibrations for unsaturated systems. The OH stretching of $–B(OH)_2$ group gives a broad peak at around 3380 cm^{-1}. The vibration of phenyl boronic acid linkage (Ph–B) gives a strong peak at 1470-1410 cm^{-1}. The absorption bands at 1342 and 1105 cm^{-1} were assigned to the vibration of the bond B–O and B–OH. The OH deformation in $–B(OH)_2$ was at 1006 cm^{-1} (Kahraman et al., 2004).

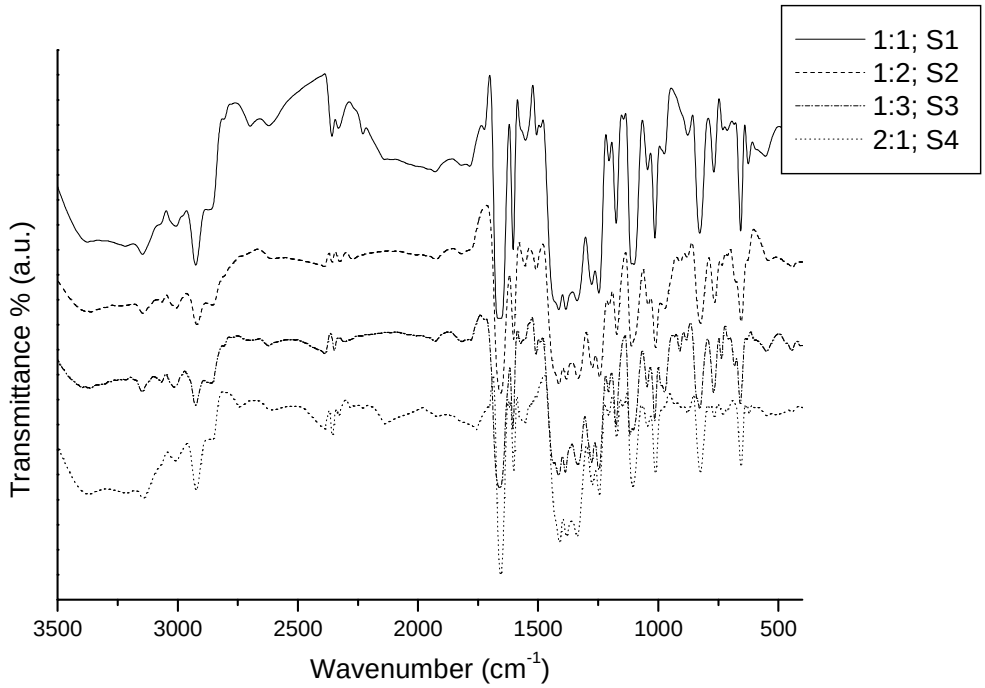

Figure 6.2. FT-IR spectra of Poly(4-VBBA-co-4-VIm) (S1, S2, S3 and S4).

After doping with H_3PO_4, three characteristic absorptions of the HPO_4^{2-}, P-OH, and $H_2PO_4^-$ groups for poly(4-VBBA-co-4-VIm) copolymer complexes appear at 1000-950 cm^{-1}. The intensity of absorption band of HPO_4^{2-} increases with increase in the concentration of H_3PO_4. The presence of HPO_4^{2-} and $H_2PO_4^-$ anions implies that proton conduction may occur according to the Grotthuss mechanism, which involves an exchange of protons between ionized phosphoric acid (Fig. 6.3). Hydrogen bond formation between aryl-N-H and aryl-N in the solid-state results in a band broadening at 3200 cm^{-1} (Colthup et al., 1990) and HPO_4^{2-} or $H_2PO_4^-$ (Rikukawa M. and K. Sanui, 2000).

The broad band between 2500-3000 cm^{-1} is attributed to the P-OH bending of the phosphoric acid (Bouchet R. and Siebert E., 1999). The frequencies and assignments of several characteristic vibrations of the copolymers are reported in Table 6.1.

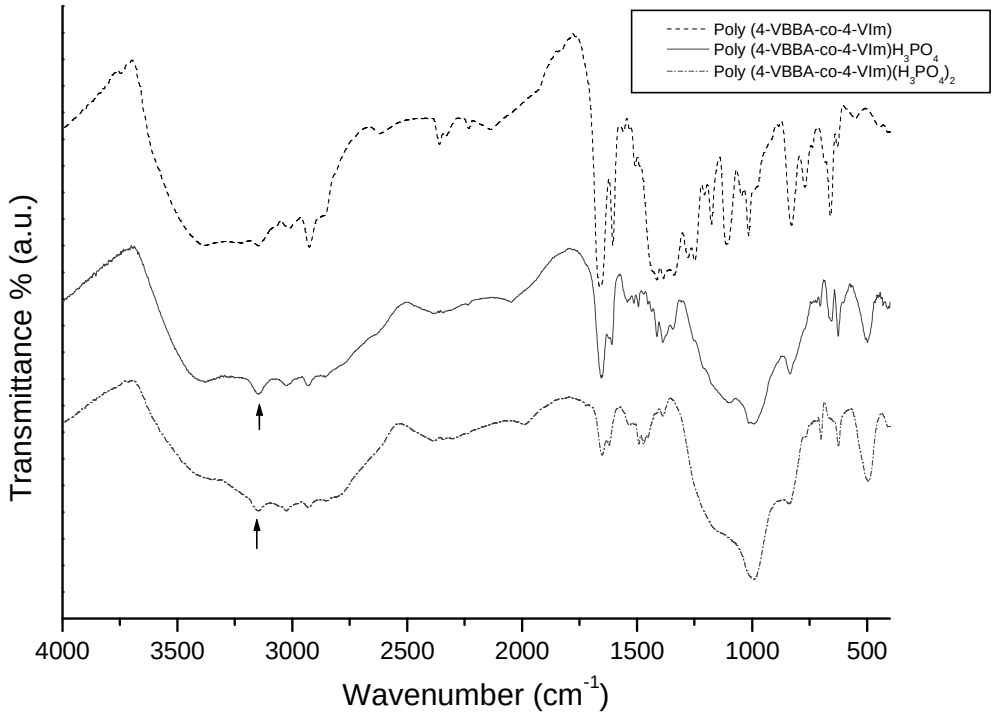

Figure 6.3. FT-IR spectra of Poly(4-VBBA-co-4-VIm) S1 and doped samples Poly(4-VBBA-co-4-VIm)$(H_3PO_4)_x$.

Table 6.1. The data of FT-IR spectra of Poly(4-VBBA-co-4-VIm) and phosphoric acid doped sample Poly(4-VBBA-co-4-VIm)$(H_3PO_4)_x$

Poly(4-VBBA-co-4-VIm) (cm^{-1})	**Poly(4-VBBA-co-4-VIm)$(H_3PO_4)_x$ (cm^{-1})**	**Attribution**
3148	3143	N-H stretching
2965-2853	2937-2835	C-H stretching
	2300-2750	P-OH stretching
1660-1606	1690-1585	C=C stretching
1552		B-O stretching
1509	1478-1560	CH_2 stretching
1414		Ph-B stretching
1342		B-O bending
	1330-994	P-O-H stretching
1275		CH_2 wagging
1185		B-OH bending
1105		B-OH stretching
1000-900		OH deformation stretching
	890-760	OPO bending
850-700		B-OH out of plane bending
	837	$P(OH)_2$, $(H_2PO_4^-)$
656		OH bending
600-420		CH ve CH_2 bending
	497	(PO_2) $H_2PO_4^-$

6.1.3 FT-IR of Pure PGMA, Ethanolamine Modificated PGMAN and Boric Acid Doped PGMANB Samples

The IR spectra of PGMA, PGMAN and PGMANB are given in Fig. 6.4. In Fig. 6.4a, the absorption peaks at 1260 and 1730 cm^{-1} were associated with the presence of the oxirane ring and carbonyl (O-C=O) in PGMA respectively (Li et al., 2005). The functionalization of PGMA brings about not only the dissapperance of the peaks due to epoxy groups at 1340, 993, 908, and 848 cm^{-1} but also appearance of the new peaks at 1088 (δ_{OH}), 1050 (δ_{CN}), and 870 (δ_{CN}) cm^{-1} and also broad bands at 3421 cm^{-1} (O-H and N-H) (Fig. 6.4b), suggesting the successful conversion of the epoxy groups with ethanolamine (Jone Selvamalar et al., 2003; Wang et al., 2007). The absence of the peak at 968 cm^{-1} in the IR spectrum of PGMANB (Fig. 6.4c) shows the absence of tetrahedrally bonded B-O (Wang et al., 2007). A small shoulder at 3225 cm^{-1} is attributed to OH vibration of B-OH band (Shih et al., 2006). An absoption peak appeared at 662 cm^{-1} was attributed to B-O units. In addtion, The absorption bands at ~ 1040 cm^{-1} and 1331 cm^{-1} were assigned to vibration of the bond (BO-C) and to the anti-symmetric stretching vibration, respectively. The existence of B-O-B linkage was proved by the peak centered at 760 cm^{-1} (Senel et al., 2007; Pennarun and Jannasch, 2005; Barros et al., 2006; Pennarun et al., 2006).

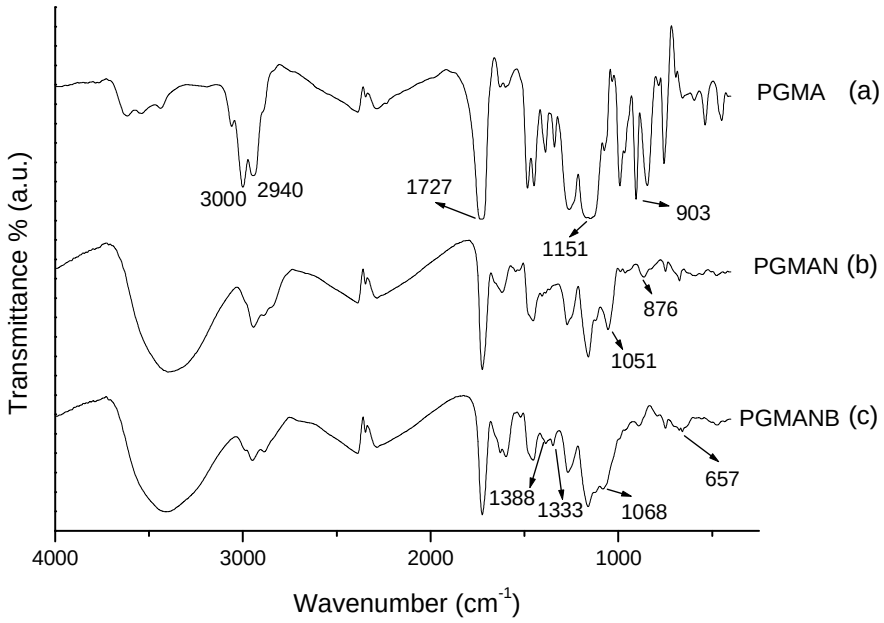

Figure 6.4. FT-IR spectra of PGMA, PGMAN and PGMANB.

6.2 X-RAY DIFFRACTION

6.2.1 X-Ray Diffraction of Poly(4-VBBA-co-4-VIm)

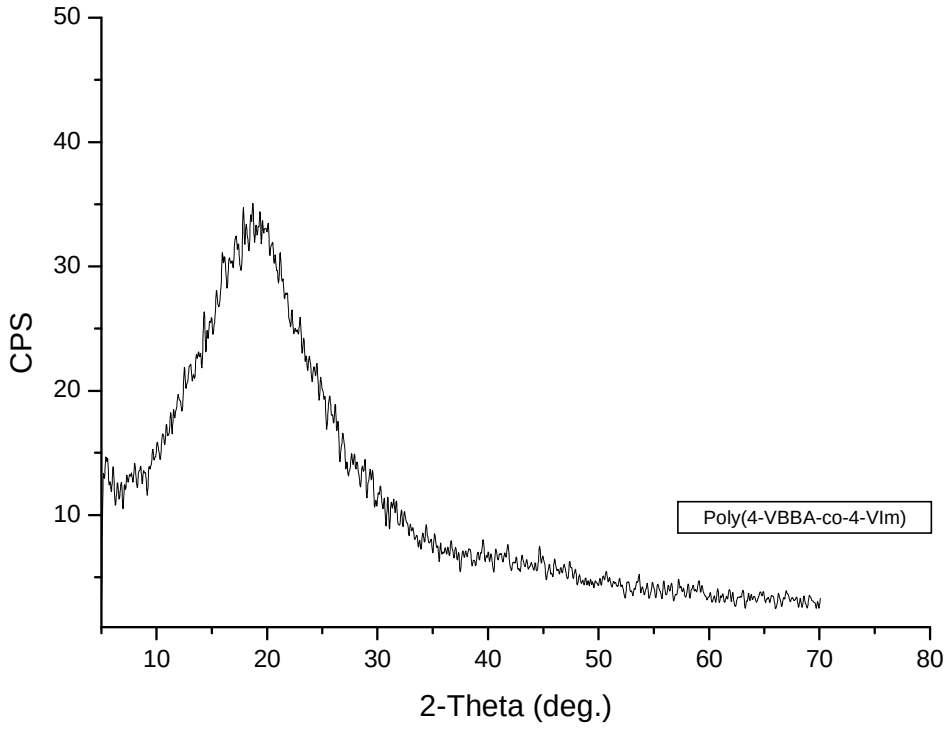

Figure 6.5. X-ray diffraction pattern of Poly(4-VBBA-co-4-VIm).

The XRD pattern of the copolymer poly(4-VBBA-co-4-VIm), S1 is presented in Fig. 6.5. The absence of a distinct diffraction pattern and the appearance of a broad hump centered around 20^{o} (2θ) can be associated with the amorphous packing of the polymer chains.

6.3 ^{13}C NMR Studies

6.3.1 ^{13}C NMR Spectra of Poly(4-VBBA-co-4-VIm)

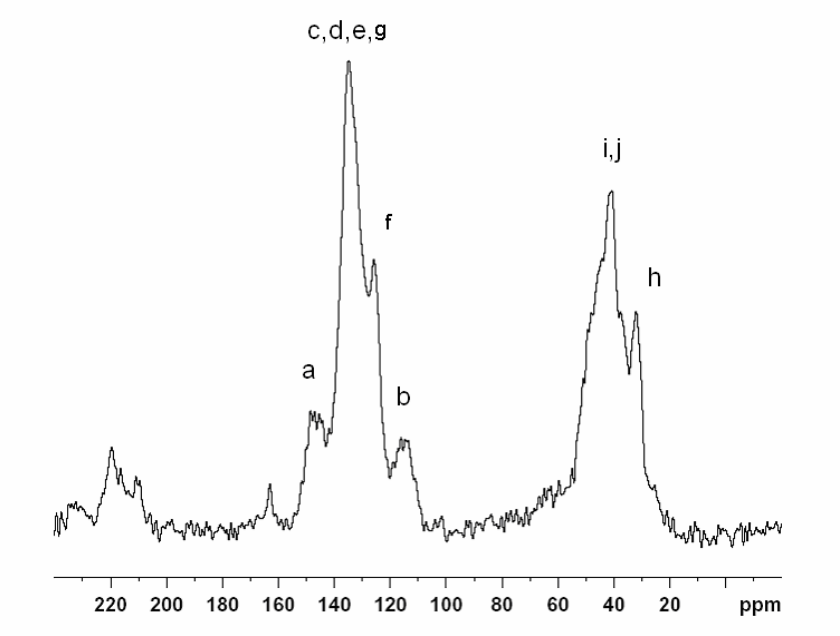

Figure 6.6. The solid ^{13}C NMR spectrum of Poly(4-VBBA-co-4-VIm) system.

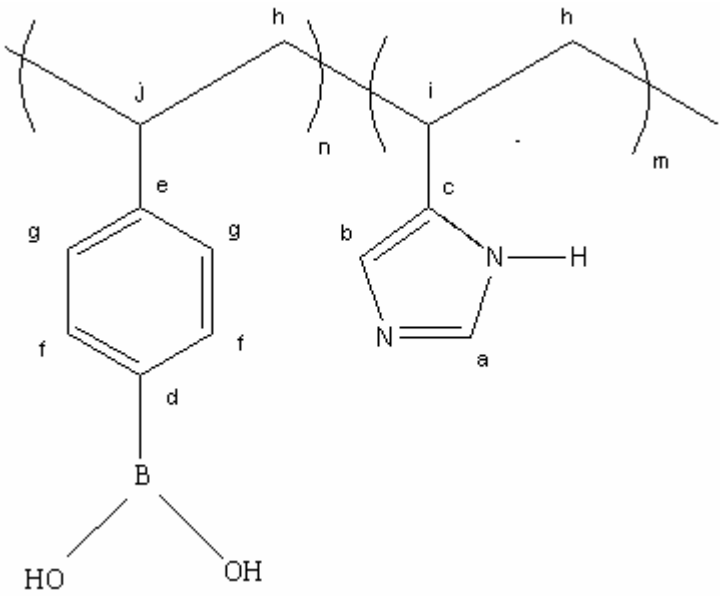

Figure 6.7. Molecular structure of Poly(4-VBBA-co-4-VIm).

The solid ^{13}C NMR spectra of poly(4-VBBA-co-4-VIm) is shown in Fig. 6.6 and Fig. 6.7, respectively. The characteristic C peaks of the imidazole rings are between 110-150 ppm and the peak located at around 130 ppm belongs to C of the benzene and imidazole groups. Signals corresponding to the methyl and methylene groups appear between 20-60 ppm.

6.4 ^{11}B MAS-NMR STUDIES

6.4.1 ^{11}B MAS-NMR Spectrum of Poly(4-VBBA-co-4-VIm)

^{11}B MAS-NMR spectrum of poly(4-VBBA-co-4-VIm) is shown in Fig. 6.8. The chemical shifts of the resonances observed are added to the figure. There are basically two separate regions where the chemical shifts are exists. Around ~2 ppm (the region specific for four-coordinated boron site), there is one resonance. In the higher chemical shifts region (17-26 ppm; region of three-coordinated boron), a more complicated pattern is observed. Due to the quadrupolar effects that broadens the peak over a large chemical shift range. One can safely say, there are at least two different boron sites contributing to this pattern. The peak at 2 ppm might be a species with four-coordination, like a free boron site in the polymer matrix. The other more crowded pattern is due to crosslinked and non-crosslinked B-$(OH)_2$.

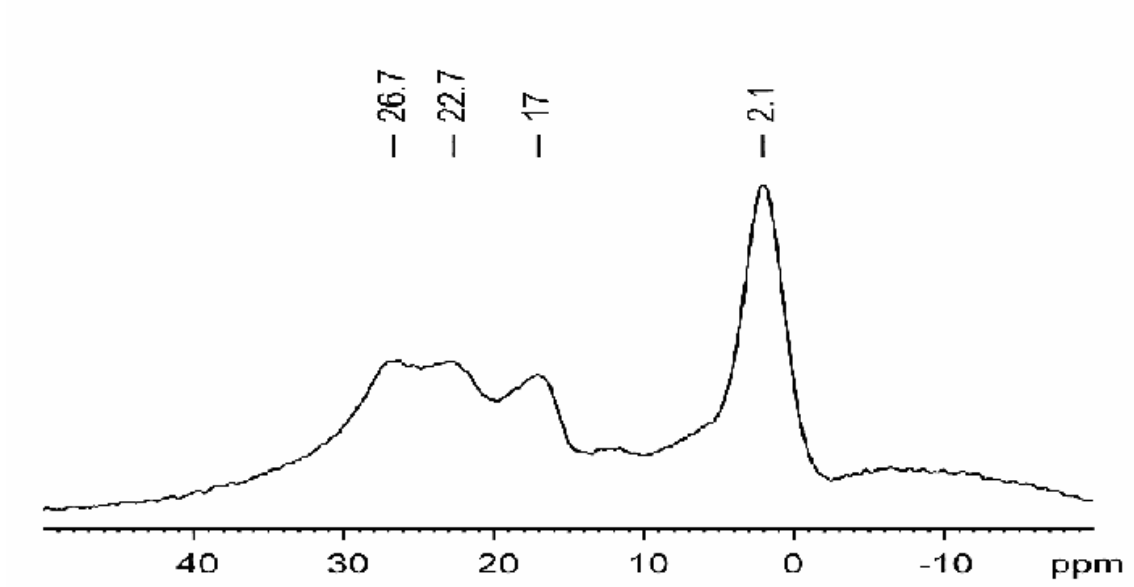

Figure 6.8. ^{11}B MAS-NMR of Poly(4-VBBA-co-4-VIm) at 15 kHz MAS frequency and at RT. The spectrum recorded at a 11.7 T magnet with a Larmor frequency of 160.46 MHz.

6.4.2 ^{11}B MAS-NMR Spectrum of PGMANB

In Fig. 6.9, ^{11}B MAS-NMR spectrum of PGMANB can be seen. From a lineshape analysis, existing of two distinct B sites can be seen manifesting itself as three resonances at 13.4 and 9 ppm. The chemical shift values are characteristic for the three-coordinated B atom. The result can be interpreted as the existing of the site as it is in the polymer, and additionally at least one more cross linked site is present. The peak at around 9 ppm is not symmetric. This feature might be due to big quadrupolar broadening of the ^{11}B atom, due to it's not 100% symmetric environment (Grimmer et al., 1997; Gervais et al., 2005). Moreover, an additional ^{11}B site with a different chemical environment (maybe a different crosslinking site) would also cause same result. At this point, this issue can not be clarified. Additional experiments need to be done to understand the system further. We can at least sure about the presence of two different ^{11}B sites in the PGMANB polymer system.

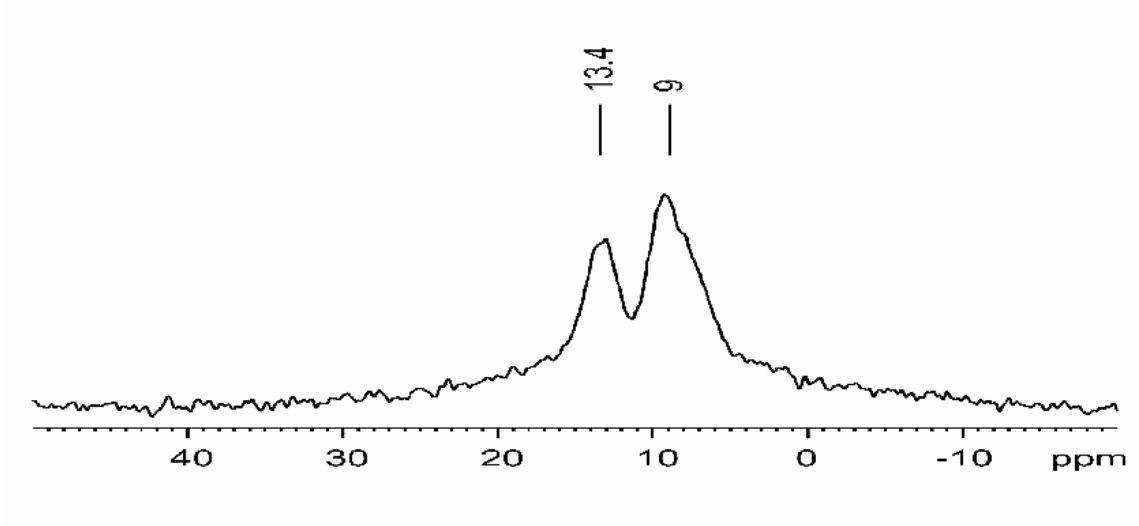

Figure 6.9. ^{11}B MAS-NMR of PGMANB at 15 kHz MAS frequency and RT. The spectrum recorded at a 11.7 T magnet with a Larmor frequency of 160.46 MHz.

6.5 THERMAL ANALYSIS

Thermogravimetric analysis has become an indispensable analytical technique for materials characterization. It involves continuous weighing of the polymer as it is subjected to a temperature program and provides quantitative and qualitative kinetic information on the degradation, oxidation, evaporation or sublimation of material under investigation (Craver, 1983). Thermogravimetric analysis is also important for compositional analysis and determination of the additives in particular. The determination of the moisture content in polymer is also possible (Wundelich, 1990; Brennan, 1977).

6.5.1 TGA of PVBBA and Doped Samples

The effect of H_3PO_4 on thermal stability of the homopolymer was investigated by Thermal Gravimetric Analysis (TGA). The phosphoric acid doped sample is stable up to 350 ^oC. TG curves of homopolymer and polymer electrolytes under N_2 atmosphere were illustrated in Fig. 6.10. TG thermograms of homopolymer shows a thermal condensation step between 100-200 ^oC .For polymer electrolytes there is a small weight loss between 150-220 ^oC which is due to water loss of B-OH group.

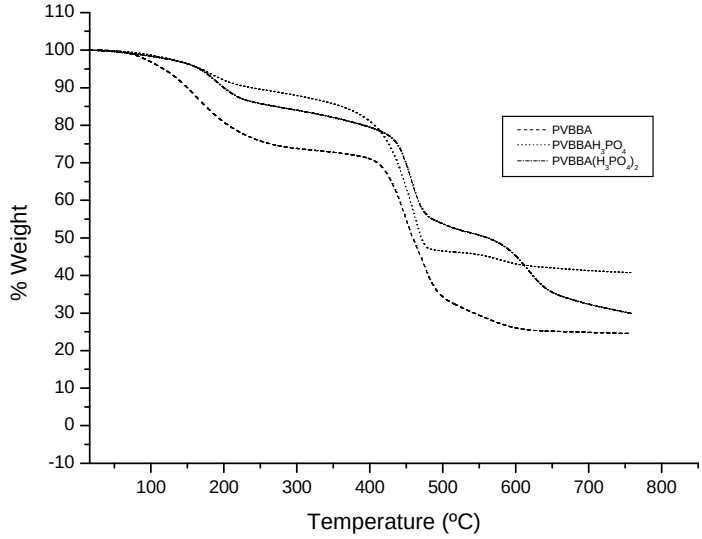

Figure 6.10. TG profiles of PVBBA, $PVBBAH_3PO_4$ and $PVBBA(H_3PO_4)_2$ under a N_2 atmosphere at a heating rate of 10 ^oC/min.

The stepwise decomposition above this temperature can be attributed to water liberation due to the self-condensation of the phosphoric acid as well as the decomposition of the polymer. The termal stability increases with doped H_3PO_4 to the homopolymer. The condensation rate decreases with increasing of acid content. The degradation of polymer begins above 350 ^oC.

6.5.2 TGA of Poly(4-VBBA-co-4-VIm) Copolymer and Doped Samples

The thermogravimetric analysis curves of the copolymer (S1) and polymer electrolytes are illustrated in Fig. 6.11. Two stages of weight loss are evident in these curves; the initial stage is from 100-200 ºC. The reason of the weight loss is thermal condensation B–OH units of the VBBA. The phosphoric acid doped sample poly(4-VBBA-co-4-VIm) has better stability and elusive exponential decay below 220 ºC may be due to evaporation of absorbed free water in these hygroscopic materials as well as removal of condensation products at higher temperatures.

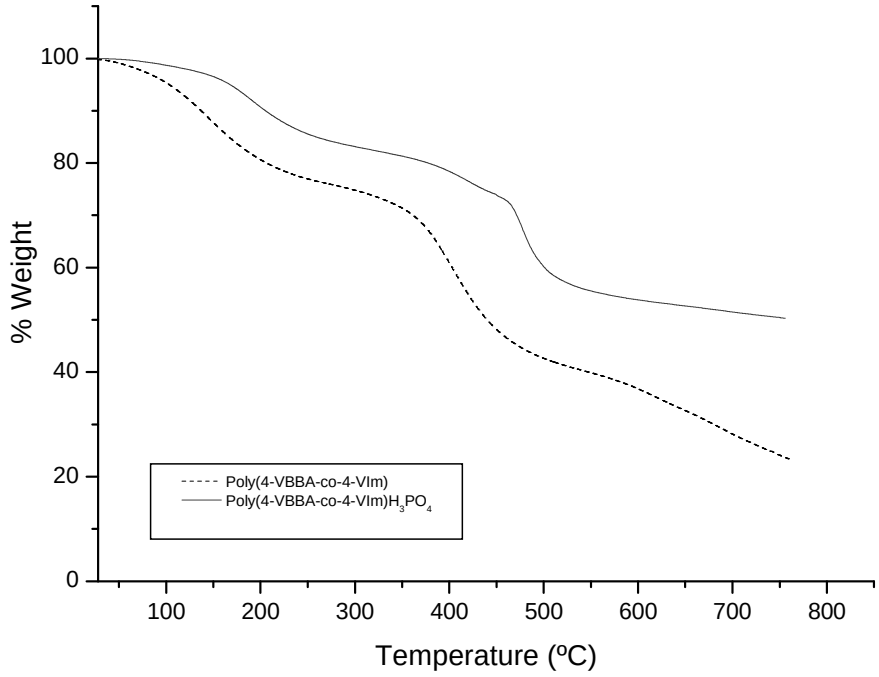

Figure 6.11. TG profiles of pure and H_3PO_4 doped Poly(4-VBBA-co-4-VIm) recorded at a heating rate of 10 ^oC/min under a nitrogen atmosphere under a N_2 atmosphere at a heating rate of 10 ^oC /min.

6.5.3 TGA Studies of PGMA

Furthermore, we carried out thermoanalytical measurements of PGMANB at heating rate of 10 ^{o}C/min. From Fig. 6.12. it can be deduced that the initial weight loss starts near 100 ^{o}C and can be attributed to evaporation of physically bound water. The decomposition of the polymer-complex above 210 ^{o}C. Nanjundan et. al reported that homopolymer PGMA is thermally stable up to 188 ^{o}C (Nanjundan et al., 2005).

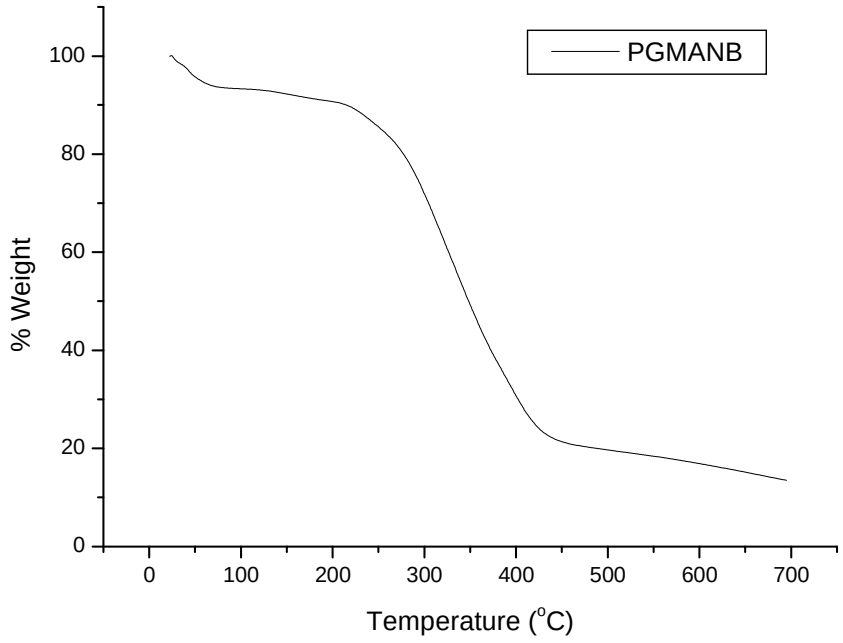

Figure 6.12. TGA curve of PGMANB recorded at a heating rate of 10 ^{o}C/min.

6.6 DIFFERENTIAL SCANNING CALORIMETRY (DSC)

Differential Scanning Calorimetry is most widely used methods of the thermal analysis in polymer science. They monitor the heat exchange can be physical or chemical in the nature. Polymerization or structural changes are almost invariably accompanied by energetic effects. Crystallization, melting, curing and other reactions, and glass transition all show characteristic DSC curves. In the DSC, small samples (a few mg) are used and rapid heating (+q), rates up to 50-100 K/min are common. This

technique is of great value for carrying out kinetic studies. Even if there are some similarities in equipment and application, DSC and DTA are different in their measurement system. In DTA, the sample and reference are heated by a single heat source with the same rate. The temperature difference between sample and reference ($\Delta T = T_s - T_r$) is measured and plotted as a function of sample temperature (T_s).The deviation of the sample temperature, T_s from T_r (ΔT) is directly proportional to the heat capacity. In DSC, the sample and reference are provided with different heaters and both sample and reference cells are kept at the same programmed temperature (T_p). The temperature of each cell is measured continuously and compared with the instantaneous value of T_p. When a sample undergoes a thermal transition, the power to the two heaters is adjusted to maintain T_p and signal proportional to the power difference is plotted versus T_p. The power difference is $W_s (T_s - T_p) - W_r (T_r - T_p)$, where the first term is the power delivered to the sample and second is power delivered to the reference (Crompton, 1989; Compbell and White, 1989).

Glass transition phenomenon manifests a transition from a glassy amorphous polymer to a flexible material on warming through T_g. At this temperature the variables entropy, S, volume, V, enthalpy, H, merely change slope with increasing temperature. Large scale segmental motions of the polymer chain occur above this temperature. The location of T_g depends on the rate at which the temperature variation is carried out.

The T_g lowering phenomenon which can occur when a nonpolymeric liquid is incorporated into some polymers is known as plasticization. The addition of nonvolatile dioctylphtalate politicizes poly(vinyl chloride) and provides a shifting of glass transition below ambient temperature (Compbell, 1994).

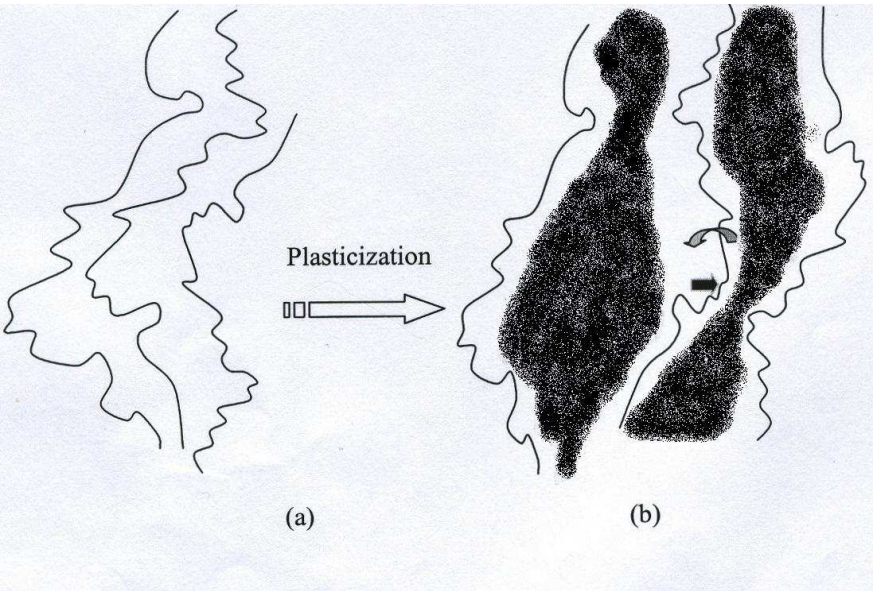

Figure 6.13. Plasticization with low molecular weight compound (Compbell, 1994).

Plasticization may be explained by a simple model shown in Fig. 6.13. The three polymer chains are close to each other as represented in the diagram by irregular lines (a). This structural feature hinders the rotation of segments of the molecular chain and increases the distance between chains, allowing chain segments to move into the space which they occupy before the liquid 'flows' into the volume from which the chain segment moves (b). The corresponding situation within the polymer is that less thermal energy in total is required to keep the segmental motion going and consequently it undergoes the transition into the glassy state at a lower T_g after plasticizer has been added.

6.6.1 DSC of PVBBA and Doped Samples

Fig. 6.14 shows the DSC thermograms of PVBBA and phosphoric acid doped samples, PVBBA$(H_3PO_4)_x$. No distinct glass transition was observed for PVBBA. However, as phosphoric acid mol ratio increases in homopolymer , T_g shifts to lower temperatures, for x = 1 Tg = 95 and for x = 2 Tg = -8 C. These results show the

plasticizing effect of phosphoric acid. Presence of a single T_g also confirms the homogeneity of these samples.

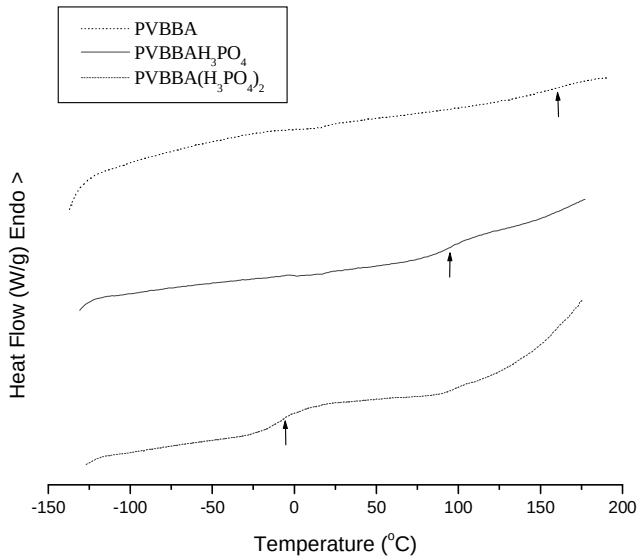

Figure 6.14. DSC thermograms of PVBBA, $PVBBAH_3PO_4$ and $PVBBA(H_3PO_4)_2$ under a N_2 atmosphere at a heating rate of 10 ^oC/min.

6.6.2 DSC of PVBBA-co-4VIm and Doped Samples

Fig. 6.15 shows the DSC thermograms of poly(4-VBBA-co-4-VIm) and phosphoric acid doped sample, poly(4-VBBA-co-4-VIm)H_3PO_4. Clearly, there is no glass transition temperature of the pristine copolymer (S1). While the phosphoric acid doped copolymer, poly(4-VBBA-co-4-VIm)H_3PO_4 has a T_g of 130 ^oC.

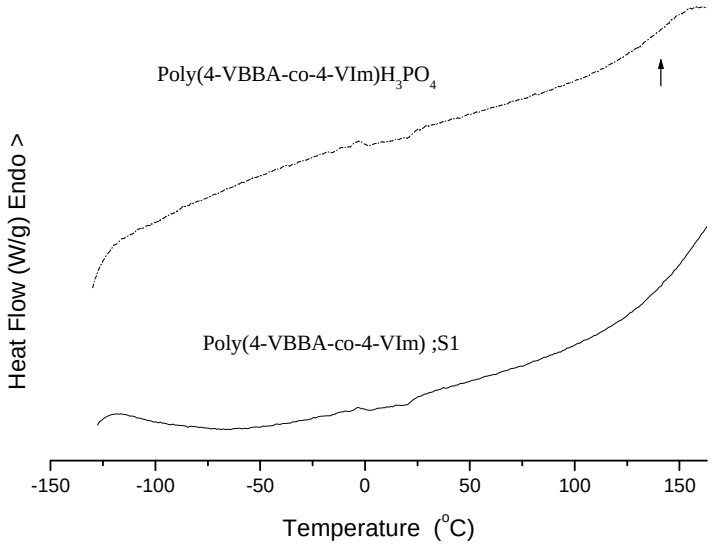

Figure 6.15. DSC thermograms of pure S1 and doped Poly(4-VBBA-co-4-VIm)x H_3PO_4 under a N_2 atmosphere at a heating rate of 10 ^oC/min.

6.7 PROTON CONDUCTIVITY

6.7.1 Conductivity of Pure and Doped PVBBA

The AC conductivities, σ_{ac} (ω) of the polymers were measured at several temperatures using impedance spectroscopy. The AC conductivity of PVBBA$(H_3PO_4)_2$ is shown in Fig. 6.17. Frequency dependent AC conductivities (σ_{ac} (ω)) were measured using Eq. 1;

$$\sigma'(\omega) = \sigma_{ac}(\omega) = \varepsilon''(\omega)\,\omega\,\varepsilon_o \qquad (1)$$

where σ' (ω) is the real part of conductivity, $\omega = 2\pi f$ is the angular frequency, εo is the vacuum permittivity ($\varepsilon_o = 8.852 \times 10^{-14}$ F/cm), and ε'' is the imaginary part of complex dielectric permittivity (ε^*).

The DC conductivity (σ_{dc}) of the samples was derived from the plateaus of log σac vs. log F by linear fitting of the data. The first irregularities at low frequency ($f<10^4$) zone are due to the blocking electrode polarizations.The platea is indicated the DC conductivity that is free to frequency. The second irregularities at high frequency zone are due to the dispersion.

The DC conductivities of the phosphoric acid doped samples were compared in Fig. 6.18. The conductivity isotherm illustrates that the DC conductivity strongly depends on temperature and the doping ratio, x. Generally, phosphoric acid doped systems exhibit Arrhenius behavior at lower acid contents and Vogel-Tamman–Fulcher-type (VTF) behavior at higher acid ratio x. For PVBBA$(H_3PO_4)_2$ (Fig. 6.18), the conductivity isotherm can be fitted by Arrhenius equation (Eq. 2);

$$\ln \sigma = \ln\sigma_o - Ea/kT \qquad (2)$$

where σ_o is the pre-exponential terms, Ea is the activation energy, and k is the Boltzmann constant.

If the system follows VTF behavior the curved DC conductivity isotherm can be fitted by VTF equation (Eq. 3);

$$\log \sigma = \log \sigma_o - E_v/[k(T-T_o)] \qquad (3)$$

where σ_o is the conductivity at infinite temperature, E_v is the Vogel activation energy and T_o is the Vogel temperature.

A linear relationship is observed in the log relaxation times of PVBBA$(H_3PO_4)_x$ versus 1000/T (Fig. 6.16 and Fig. 6.17). The activation energy was found to be E_a = 0,0175 KJ/mol when the doping ratios x = 1 and x = 2.

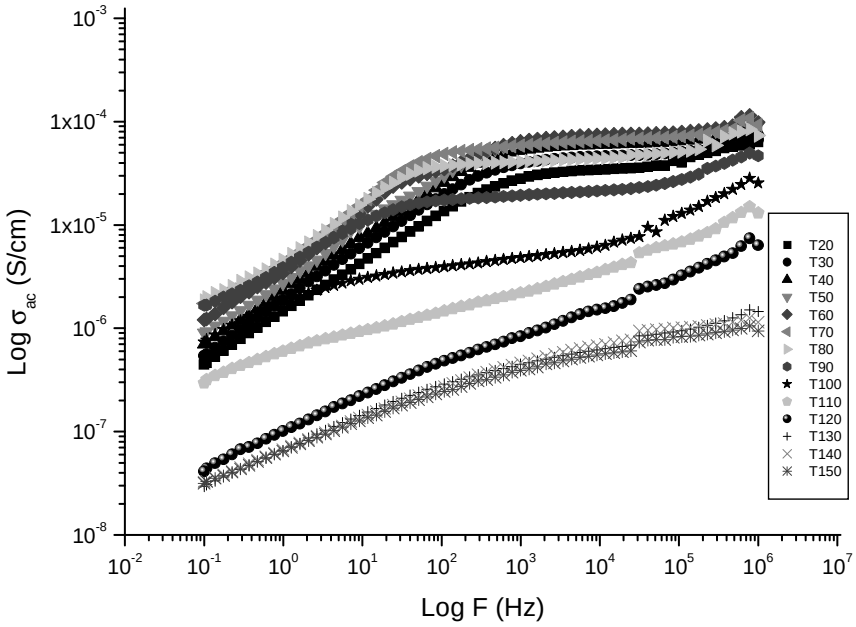

Figure 6.16. AC conductivity versus Frequency (Hz) for $PVBBAH_3PO_4$ at various temperatures.

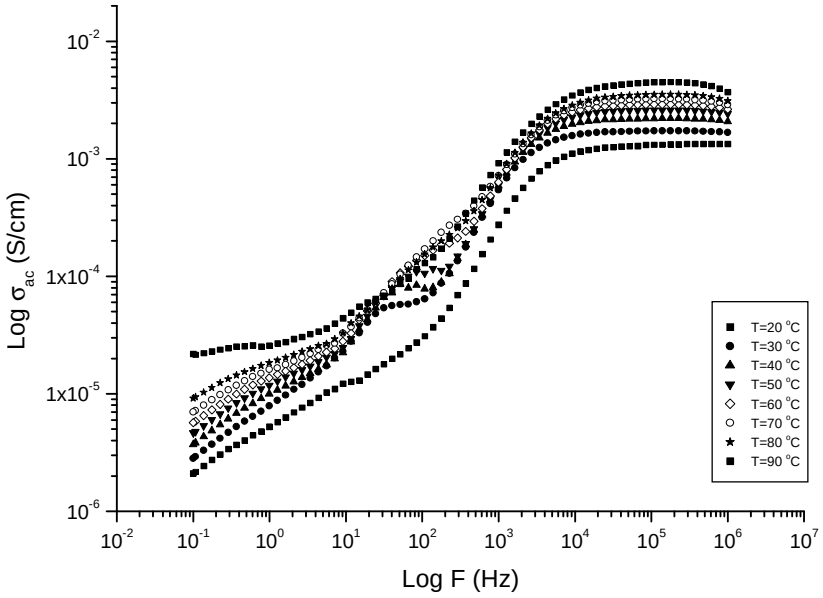

Figure 6.17. AC conductivity versus Frequency (Hz) for $PVBBA(H_3PO_4)_2$ at various temperatures.

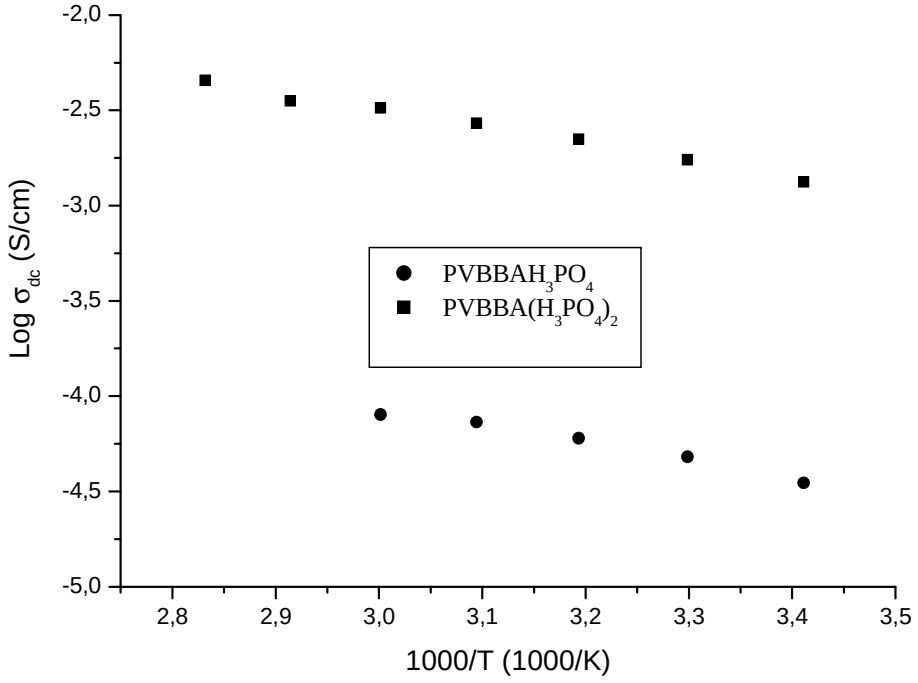

Figure 6.18. DC conductivities of $PVBBAH_3PO_4$ and $PVBBA(H_3PO_4)_2$ as a function of reciprocal temperature.

6.7.2 Conductivity of Poly(4-VBBA-co-4-VIm) and Doped Samples

The temperature dependences of the proton conductivity of copolymer and acid doped samples are illustrated in Fig. 6.19-6.21. All the electrolytes showed a positive temperature-conductivity dependency within the temperature range of measurements. The conductivity isotherm shows Arrhenius behaviour at higher acid composition. Clearly, the proton conductivity slightly changes within the given temperature range (20-100 ^oC) for poly(4-VBBA-co-4-VIm)H_3PO_4 and slightly increases for poly(4-VBBA-co-4-VIm)$(H_3PO_4)_2$ with recpect to temperature. The reason can be described by the proton conduction over the phosphoric acid phase which is accumulated over the hydhophilic channels, i.e., boric acid, imidazole. At higher temperatures the conductivity decreases due to condensation of B-OH units which may shrink those channels and conductivity is reduced at higher temperatures (Fig. 6.21). There are mainly two transport mechanisms that contribute to the proton conductivity in phosphoric acid doped polymer electrolytes. The first is the structural diffusion

(Grotthuss mechanism) in which the conductivity is mainly controlled by proton transport through phosphate ions, i.e. $H_4PO_4^+$, $H_2PO_4^-$ (Grotthuss proton transport). The second is the vehicle mechanism where the protons travel through the material on a neutral or charged "vehicle". Several studies were reported about the contribution of these mechanisms on the proton conductivity of pure phosphoric acid and it was indicated that the character of conduction mechanism is mainly controlled by the structural diffusion rather than vehicle mechanism (Dippel et al., 1993). Additionally the proton diffusion can be can be supported by the proton transfer between imidazolium ion which is immobilized in the main chain and phosphoric acid units as in the case of PBI/phosphoric acid systems (He et al., 2003). The ionic conductivity of copolymer is low and doesn't show high difference with temperature. The conductivity of poly(4-VBBA-co-4-VIm) increases according to the temperature and it reaches the value of 5×10^{-3} S/cm at 90 ºC (Fig. 6.22).

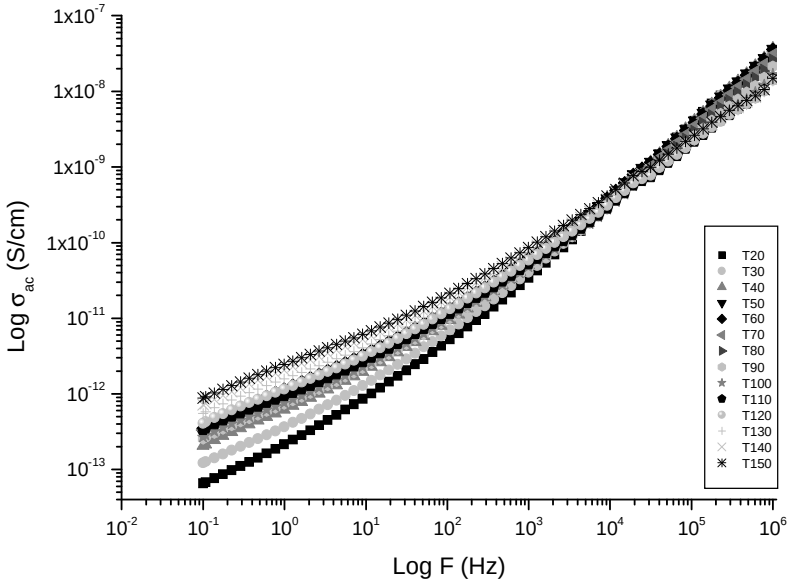

Figure 6.19. AC conductivity versus Frequency (Hz) for pure poly(4-VBBA-co-4-Vım) (S1) at various temperatures.

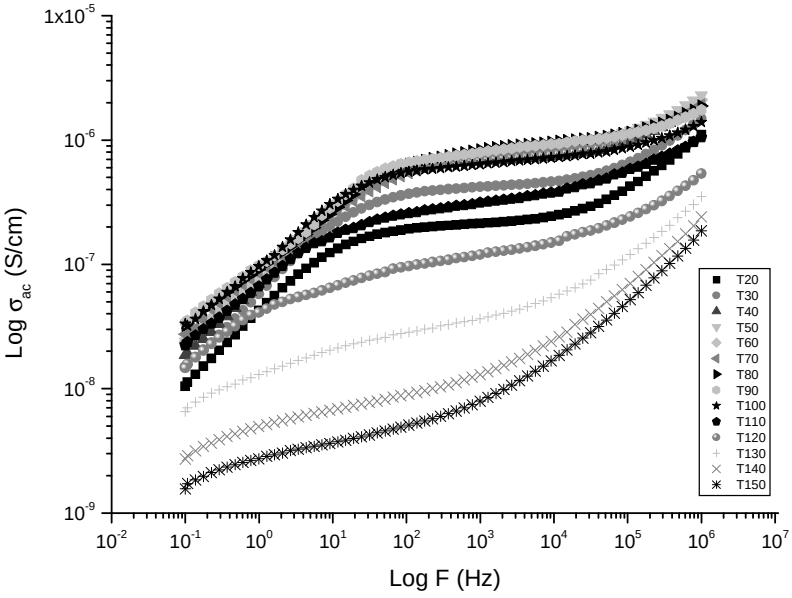

Figure 6.20. AC conductivity versus Frequency (Hz) for poly(4-VBBA-co-4-VIm) H_3PO_4 at various temperatures.

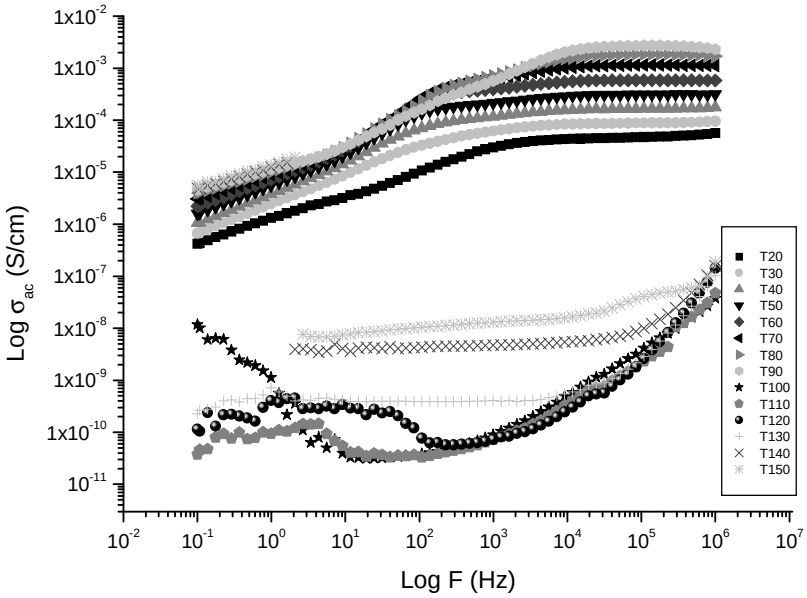

Figure 6.21. AC conductivity versus Frequency (Hz) for poly(4-VBBA-co-4-VIm) $(H_3PO_4)_2$ at various temperatures.

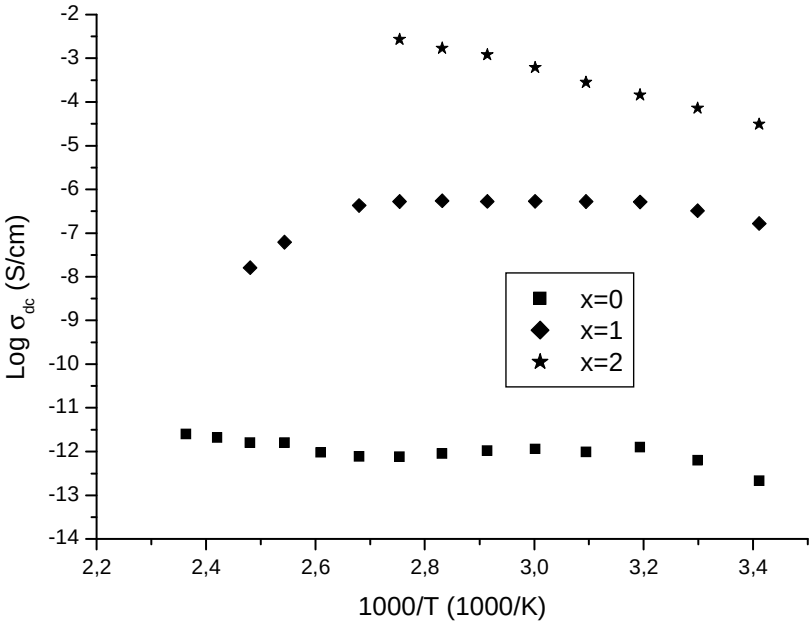

Figure 6.22. DC conductivities of the Poly(4-VBBA-co-4-VIm) S1 and doped samples Poly(4-VBBA-co-4-VIm)$(H_3PO_4)_x$ as a function of reciprocal temperature.

CHAPTER 7

CONCLUSIONS

This work focus on understanding fundamental properties of acid doped poly(4-vinylbenzeneboronic acid), PVBBA homopolymer and poly(4-VBBA-co-4-VIm) copolymers. No distinct glass transition was observed for PVBBA. However, as phosphoric acid mol ratio increases in homopolymer , T_g shifts to lower temperatures, for x = 1, T_g = 95 ^oC and for x = 2, T_g = -8 ^oC. These results show the plasticizing effect of phosphoric acid. A linear relationship is observed in the log relaxation times of PVBBA$(H_3PO_4)_x$ versus 1000/T (Fig. 6.16 and Fig. 6.17). The activation energy was found to be E_a = 0,0175 KJ/mol when the doping ratios x = 1 and x = 2. For poly(4-VBBA-co-4-VIm) there is no glass transition temperature of the pristine copolymer (S1). While the phosphoric acid doped copolymer, poly(4-VBBA-co-4-VIm)H_3PO_4 has a T_g of 130 ^oC. From ^{11}B MAS-NMR spectrum of poly(4-VBBA-co-4-VIm), we can safely say there are at least two different boron sites contributing to this pattern. The peak at 2 ppm might be a species with four-coordination, like a free boron site in the polymer matrix. The other more crowded pattern is due to, crosslinked and non-crosslinked B-$(OH)_2$. The conductivity of doped sample reaches the value of 5 x 10^{-3} S/cm at 90 ^oC.

The proton conductivity slightly changes within the given temperature range (20-100 ^oC) for poly(4-VBBA-co-4-VIm)H_3PO_4 and slightly increases for poly(4-VBBA-co-4-VIm)$(H_3PO_4)_2$ with respect to temperature. The reason can be described by the proton conduction over the phosphoric acid phase which is accumulated over the hydrophilic channels, i.e., boric acid, imidazole. At higher temperatures the conductivity decreases due to condensation of B-OH units which may shrink those channels and conductivity is reduced at higher temperatures. The conductivity of

poly(4-VBBA-co-4-VIm) increases according to the temperature and it reaches the value of 3×10^{-3} S/cm at 98 ºC.

Poly(glycidyl methacrylate) (PGMA) was synthesized via radical polymerization of glycidyl methacrylate (GMA) initiated by AIBN and followed by modification of with ethanolamine. Borate-loaded PGMAN (PGMANB) complexes were prepared by mixing PGMAN and boric acid solution in a molar ratio of 1:1. PGMANB was investigated by FT-IR spectroscopy, elemental analysis and ^{11}B MAS-NMR to confirm the structure and its thermal properties were studied by thermogravimetry analysis. For these complex the initial weight loss starts near 100 ^{o}C and can be attributed to evaporation of physically bound water. The decomposition of the polymer-complex above 210 ^{o}C. In ^{11}B MAS-NMR spectrum of PGMANB, there are three-coordinated B atom. We can at least sure about the presence of two different ^{11}B sites in the PGMANB polymer system.

REFERENCES

Adhikiri D.P., M.D. Heagy, *Tetrahedron Lett.*, Vol. 40, pp. 7893, 1999.

Akita H., M. Ichikawa, K. Nosaki, H. Oyanagi, and M. Iguchi, *U.S. Patent*, Vol. 6, pp. 124.060, 2000.

Aoki T., Y. Nagao, K. Sanui, N. Ogata, A. Kikuchi, Y. Sakurai, K. Kataoka, T. Okano, *Polym. J.*, Vol. 28, pp. 371, 1996.

Appleton B., T.D. Gibson, *Sens. Actuators B*, Vol. 65, pp. 302, 2000.

Barros P.M., I. Valeria, P. Yoshida, Marco A. Schiavon, *Journal of Non-Crystalline Solids*, Vol. 352,pp. 3444-3450, 2006.

Bermudez V.D., M. Armand, C. Poinsignon, L. Abello, and J. Y. Sanchez, *Electrochim. Acta*, Vol. 37, pp. 1603, 1992.

Blomen L.J.M.J. and M.N. Mugerwa, Editors, *Fuel Cell Systems*, Plenum Press, New York, 1993.

Bouchet R., E. Siebert, *Solid State Ionics*, Vol. 118, pp. 287-299, 1999.

Bozkurt A., W.H. Meyer, G.. Wegner, *Journal of Power Sources*, Vol. 123, pp. 126, 2003.

Bozkurt A., M. Ise, K.D. Kreuer, W.H. Meyer, G.. Wegner, *Solid State Ionics*, Vol. 125, pp. 225-233, 1999.

Bozkurt A., W.H. Meyer, *Journal of Polymer Science: Part B: Polymer Physics*, Vol. 39, pp. 1987-1994, 2001b.

Bozkurt A. , W.H. Meyer, Solid State Ionics, Vol. 138, pp. 259-265, 2001a.

Bozkurt A., W. H. Meyer, and G. Wegner, *J. Power Sources* Vol. 123, pp. 126, 2003.

Cabell L.A., M.K. Monahan, E.V. Anslyn, *Tetrahedron Lett.*, Vol. 40, pp. 7753, 1999.

Camli S.T., M. Tuncel, S. Senel, A. Tuncel, *J. Chromatogr. B*, Vol. 769, pp. 283, 2002.

Canizzo C., S.A. Gerbier, C. Larpent, *Polymer,* Vol. 46, pp. 1269, 2005.

Chin D.T., H.H. Chang,. *J. Appl. Electrochem.*, Vol. 19, pp. 95-99, 1989.

Compbell I.M., *Introduction to Synthetic Polymers*, Oxford University Press, 1994.

Colthup N.B., L.H. Daly, S.E. Wiberty, *Introduction to Infrared Raman Specroscopy*, Academic Press, New York, 1990.

Cremers C., U. Stimming, Low Temperature Fuel Cells: Development Status and Future Perspectives, , *International Union of Pure and Applied Physics*, Annex A, V- Fuel Cells, pp. 234, 2004

Decoursey T. E., *Phys. Rev.*, Vol. 83, pp. 475, 2003.

Dippel T., K.D. Kreuer, J.C. Lass`egues, D. Rodriguez, *Solid State Ionics*, Vol. 61, No.1-3, pp. 41–46, 1993.

Donoso P., W.Gorecki, C. Berthier, F. Defendini, C. Poinsignon, M.B. Armand, *Solid State Ionics,*Vol. 28/30, pp. 969-974, 1988.

Elmas B., M.A. Onur, S. Senel, A. Tuncel, *Colloids Surf. A*, Vol. 232, pp. 253, 2004.

Erdemi H., A. Bozkurt, W.H. Meyer, *Synthetic Metals*, Vol. 143, pp. 133-138, 2004.

Frankland E., B.F. Duppa, Justus Liebigs *Ann. Chem*., Vol. 115, pp. 319, 1860.

Fuell Cell Hand Book, Parsons Inc., West Virginia, 2000.

Gabai R., N. Sallacan, V. Chegel, T. Bourenko, E. Katz and I. Willner, *J. Phys. Chem. B*, Vol. 105, pp. 8196-8202, 2001.

Gao S., W. Wang, B. Wang, *Bioorg. Chim*., Vol. 29, pp.308, 2001.

Gardiner S., B. Smith, P. Duggan, M. Karpa, G. Griffin, *Tetrahedron*, Vol. 55, pp. 2857, 1999.

Gavach C., and G.. Pourcelly, *in Proton Conductors, (Edited by Ph. Colomban),* pp. 487, Cambridge University Press, 1992.

Gervais C., E. Framery, C. Duriez, J. Maquet, M. Vaultier, *Florence Babonneau Journal of the European Ceramic Society*, Vol. 25, pp. 129-135, 2005.

Grimmer A.R., D. Müller, G. Gözel, R. Kniep, Fresenius *J. Anal. Chem*., Vol. 357, pp. 485-488, 1997.

Hall D.G.., *Boronic acid: Preparation, Application in Organic Synthesis Medicine*, Chapter 1, Weinheim, 2005.

He R., Q. Li, G. Xiao, N. J. Bjerrum, *J. Mem. Sci.*, Vol. 226, pp. 169-184, 2003.

Hickman B.S., M. Mascal, J.J. Titman, I.G. Wood, *J. Am, Chem. Soc*., Vol. 121, pp.11486, 1999.

Hisamitsu I., K. Kataoka, T. Okano, Y. Sakurai, *Pharm. Res*., Vol.14, pp. 289, 1997.

Hoel D., E. Grunwald, *J. Phys. Chem.*, Vol. 81, pp. 2135, 1977.

James T.D., K.R.A.S. Sandanayake, R. Iguchi, S. Shinkai, *J. Am. Chem. Soc.*, Vol. 117, pp. 8982, 1995.

Kahraman G., O.Beşkardeş, Z.M.O. Rzaev, E.Pişkin, *Polymer*, Vol. 45, pp. 5813-5828, 2004.

Karadedeli B., A. Bozkurt, A. Baykal, *Physica B*, Vol. 364, pp. 279-284, 2005.

Kataoka K., H. Miyazaki, T. Okano, Y. Sakurai, *Macromolecules*, Vol. 27, pp. 1061, 1994.

Kawada A., A. R.McGhie, M. M.Labes, *J. Chem. Phys.*, Vol. 52, pp. 3121, 1970.

Kim J.,T. Mori,S. Hayashi, and I. Honma, *Journal of The Electrochemical Society,Vol.* 154, pp. A290-A294, 2007.

Kitano H., N. Kuwayama, K. Ohno, *Langmuir*, Vol. 14, pp. 165, 1998.

Koyama T., K. Terauchi, *J. Chromatogr. B*, Vol. 679, pp. 31, 1996.

Kreuer K.D., A. Fuchs, M. Ise, M. Spaeth, and J. Maier, *Electrochim. Acta*, Vol. 43, (10-11), pp.1281, 1998.

Kreuer K.D., *Chemistry Materials*, Vol. 8, pp.610-641, 1996.

Kreuer K.D., *Solid State Ionics: Science & Technology*, pp. 263, 1998.

Kreuer K.D., W. Weppner, A.Rabenau, *Angew. Chem., Int. Ed.*, Vol. 21, pp. 208, 1982.

Kreuer K.D., *Solid State Ionics*, Vol. 136-137, pp. 149-60, 2000.

Kreuer S., J. Paddison, E. Spohr, M. Schuster, *Chem. Rev.*, Vol. 104, pp. 4637-4678, 2004.

Kreuer K.D., *J. Membrane Sci*., Vol. 185, pp. 29-39, 2001.

Kreuer K.D., Th. Dippel, W. H. Meyer, J. Maier, *Mat. Res. Soc. Symp. Proc*., Vol. 293, pp. 273-282, 1993.

Lassegues J.C., J. Grondin, M. Hernandez, B. Maree, *Solid State Ionics*, Vol. 145(1-4), pp. 37–45, 2001.

Lassegues J.C., *Proton Conductors, Solids Membranes, and Gels-Materials and Gels-Materials and Devices, ed. P.Colomban*, Cambridge University Press, Cambridge, pp. 311-328, 1992.

Li G., X. Zhu , J. Zhu, Z. Cheng, W. Zhang, *Polymer*, Vol. 46, pp. 12716-12721, 2005.

Li Q. F., R.H. He, J.A. Gao, J.O. Jensen, N.J. Bjerrum, *J. Electrochem. Soc*., Vol. 150, (15), pp. A1599-A1605, 2003.

Ma Y., *The fundamental Studies of Polybenzimidazole/Phosphoric Acid Electrolyte for Fuel*, Ph. D Thesis, Case Westhern Reserve University, 2004.

Miyatake K., E. Shouji, K. Yamamoto, E. Tsuchida, *Macromolecules*, Vol. 30, pp. 2941, 1997.

Nanjundan S., C. Sreekuttan Unnithan , C.S. Jone Selvamalar , A. Penlidis , *Reactive & Functional Polymers*, Vol. 62, pp. 11–24, 2005.

Overberger C.G., N. Vorchheimer, *J. Am. Chem. Soc*., Vol. 85, pp. 951, 1963.

Pennarun O.Y., P. Jannasch, *Solid State Ionics,* Vol. 176, pp. 1103-1112, 2005.

Pennarun P.Y., P.Jannasch, S. Papaefthimiou, N. Skarpentzos, P. Yianoulis, *Thin Solid Films*, Vol. 514, pp. 258-266, 2006.

Petty-Week S., J.J. Zupancic, J.R. Swedo, *Solid State Ionics*, Vol. 31, pp. 117-125, 1988.

Przyluski J. and W. Wieczorek, *Synthetic Metals*,Vol. 45, pp. 323-333, 1991.

Pu H., *Polym Int.,* Vol. 52, pp.1540-1545, 2003.

Pu H., W.H. Meyer, G. Wegner, *Journal of Polymer Science: Part B: Polymer Physics*,Vol. 40, pp. 663-669, 2002.

Pu H., W.H. Meyer, G.. Wegner, *Macromol.Chem.Phys*., Vol. 202, pp. 1478-1482, 2001.

Rettig S.J., J. Trotter, *Can. J. Chem*., Vol. 55, pp. 3071-3075, 1977.

Rikukawa M., D. Inagaki, K. Kaneko, Y. Takeoka, I. Ito, Y. Kanzaki and K. Sanui,J. Molecular Strucrure, Vol. 736, pp. 153-161, 2005.

Rikukawa M. and K.Sanui, *Prog.Polym*., Vol. 25, pp. 1463-1502, 2000.

Rodriguez D., C. Jegat, O. Trinquet, J. Grondin, J.C. Lassegues, *Solid State Ionics*, Vol. 61, pp. 195-202, 1993.

Samms S.R., S. Wasmus, R.F. Savinell, *J. Electrochem. Soc.,* Vol. 143, pp. 1225-1232, 1996.

Savinell R., E. Yeager, D. Tryk, U. Landau, J. Wainright, D. Weng, K. Lux, M. Litt, and C. Rogers, *J. Electrochem. Soc.*, Vol. 141, No. 4, 1994.

Schuster M. F. H., W.H. Meyer, *Annu. Rev. Mater. Res*., Vol. 33, pp. 233-261, 2003.

Selvamalar C.S. J., T. Krithiga, A. Penlidis, S. Nanjundan, *Reactive&Functional Polymers*, Vol. 56, pp. 89-101, 2003.

Senel M., A. Bozkurt , H. Baykal, *IONICS (International Journal of Ionics Science & Technolojy of Ionic Motion),* Vol. 13, pp. 263-266, 2007.

Shih C.C., K.H. Wu, G.P. Wang, T.R. Wu, T.C.Chang, *Polymer Degredation and Stability*, Vol. 91, pp. 1658-1664, 2006.

Shiino D., Y. Murata, A. Kubo, Y.J. Kim, K. Kataoka, Y. Koyama, A. Kikuchi, M. Yokoyama, Y. Sakurai, T. Okano, *J. Control Release,* Vol. 37, pp. 269, 1995.

Shiomori K., A.E. Ivanov, I.Y. Galaev, Y. Kawano, B. Mattiasson, *Macromol. Chem. Phys.*, Vol. 205, pp. 27, 2004.

Slaiti P., F. Lufrano, A.S. Arico, E. Pasalacqua, and V. Anolonucci, *J. membr. Sci.*, Vol. 188, pp. 71, 2001.

Slaiti P., M. Minuloli, and S. Hocevar, *J. Power Sources***,** Vol. 90, pp. 231, 2000**.**

Spaeth M., K.D. Kreuer, T. Dippel, J. Maier, *Solid State Ionics*, Vol. 97, pp. 291, 1997.

Spaeth M., K. D. Kreuer, J. Maier, *J. Solid State Chem*., Vol.148, pp. 169, 1999.

Springsteen G., and B. Wang, *Tetrahedron,* Vol. 58, pp. 5291, 2002.

Senel M., A. Bozkurt, A. Baykal, *Ionics*, Vol. 13, pp. 263-266, 2007.

Sukumar P.R., *New Proton Conducting Membranes for Fuel Cell Applications,* Ph.D. Thesis, Johannes Gutenberg University, Mainz, 2006.

Tatara W., M.J.Wojcik, , J. Lindgren, M. Probst, *J. Phys. Chem. A*, Vol. 107, pp. 7827, 2003.

Toda F., K. Tanaka, C. Foces-Foces, A. L. Llamas-Saiz, H.H. Limbach, F. Aguilar-Parrilla, R. M. Claramunt, C. Lo´pez, J. Elguero, *J. Chem. Soc. Chem. Commun.*, pp. 1139, 1993.

Tong A.J., A. Yamauchi, T. Hayashita, Z.Y. Zhang, B.D. Smith, N. Teramae, *Anal. Chem*., Vol. 73, pp. 1530, 2001.

Tuncel A., A. Ozdemir, *J. Biomater. Sci-Polym. E*., Vol. 11, pp.817, 2000.

Uguzdogan E., E.B. Denkbas, A. Tuncel, *Macromol. Biosci.*, Vol. 2, pp. 214, 2002.

Uguzdogan E., H. Kayi, E.B. Denkbas, A. Tuncel, *Polym. Int.*, Vol. 52, pp. 649, 2003.

Wainrigh J.S., J.T. Wang, R.F. Savinell, M. Litt, H. Moadell, C. Rogers, *Proc. ECS 94/23, Electrode Materials and Processes*, pp. 255, 1994.

Wainright J.S., J.T. Wang, D. Weng, R.F. Savinell, and M. Litt, *J. Electrochem. Soc.*, Vol. 142, pp. L121, 1995.

Wang L., T. Qi , Z. Gao , Y. Zhang , J. Chu , *Reactive & Functional Polymers,* Vol. 67, pp. 202-209, 2007.

Xing B., and O. Savadogo, *J.New Mater. Electrochem. Syst.*, Vol**.** 2, pp. 95, 1995.

Xing B., and O. Savadogo, *Electrochem. Commun.*, Vol. 2, pp. 697, 2000.

Yamamato M., M. Takeuchi, S. Shinkai, *Tetrahedron,* Vol. 54, pp. 3125, 1998.

Zhai Y., H. Zhang, Y. Zhang, D. Xing, *Journal of Power Sources,* Vol. 169, pp. 259-264, 2007.

Zundel G.., and E.G.. Weidemann, *Eur. Biophys. Congr., Proc., 1st,* Vol. 6, pp. 43, 1971.